Network Inference And Graph Learning in Characterizing Seizure Dynamics from EEG Signals

by

Wei Cao

A thesis submitted to the
Department of Computer Science
in conformity with the requirements for
the degree of Master of Science

Bishop's University
Canada
January 2026

Abstract

This research aims to enhance seizure detection from EEG recordings using Wavelet Tools and Graph Neural Networks (GNNs). EEG signals are inherently non-stationary and complex, rendering traditional analysis methods less effective. Wavelet transforms provide a multi-resolution analysis, capturing both time and frequency information, which is crucial for identifying transient events like seizures. By utilizing cross-spectrum and bispectrum analysis, this work extracts both linear and nonlinear connectivity features to reveal dynamic interactions across brain regions and frequency bands. While Within Frequency Coupling (WFC) and Cross Frequency Coupling (CFC) have proven to be promising features for seizure detection in conventional machine learning approaches, these methods heavily rely on manual feature extraction. In contrast, Deep Learning methods can automatically learn representations from raw data. However, traditional architectures like CNNs and RNNs often struggle to capture the complex, multi-contextual relationships inherent in EEG data. Building upon state-of-the-art GNN models, we propose a unified network design that integrates spatial, temporal, and semantic information. We explore various message-passing and aggregation architectures within spectral GNNs to develop an optimal structure for seizure detection. The proposed framework is evaluated on the Temple University Hospital Seizure (TUSZ) Corpus, comparing its performance against existing methods using metrics such as AUROC and recall. Results demonstrate the superior performance of the Graph Wavelet Neural Network and suggest the importance of proper scale parameter selection.

Acknowledgments

I would like to express my sincere gratitude to the many individuals who have helped and supported me throughout the completion of this thesis.

First, I would like to offer my deepest thanks to my supervisor, Dr. Rachid Hedjam. From the initial selection of my topic and research direction to the review of the final draft, Dr. Hedjam provided patient and meticulous guidance. His rigorous approach to scholarship, profound professional knowledge, and sharp insights have been of immense benefit to me during my Master's studies.

I also extend my heartfelt gratitude to my co-supervisor, Professor Bessam Abdulrazak of the AMI Lab at Université de Sherbrooke. I am grateful for his crucial mentorship and for the valuable internship opportunity he provided. I would also like to thank my colleagues at the AMI Lab; our discussions offered great inspiration, and their kind assistance was essential to the success of this research.

Furthermore, this work was made possible by generous financial support from Bishop's University, including the 2024-2025 Graduate Entrance Scholarship, the 2025 Drew MacCannell Award for Interdisciplinary Excellence, and the 2025 B.E.S.T. Fund. Without this funding, this research would have been difficult to conduct.

Finally, I must thank my family and friends, who have always been my strongest supporters. I am grateful for their understanding and constant encouragement throughout my Master's program.

Contents

List of Tables

List of Figures

Chapter 1

Introduction

1.1 Background

A seizure is defined as a sudden, paroxysmal alteration in neurological function caused by the excessive and hypersynchronous discharge of neurons in the brain. It manifests through changes in motor, sensory, autonomic, or cognitive functions, depending on the brain regions involved [63]. Epilepsy is defined by the International League Against Epilepsy (ILAE) as a condition characterized by a pathological and enduring tendency for recurrent seizures. Diagnosis requires either two unprovoked seizures more than 24 hours apart, one unprovoked seizure with a $\geq$60% recurrence risk over 10 years, or the presence of an epilepsy syndrome [12]. Seizures can occur independently or as part of epilepsy, but epilepsy always includes recurrent seizures as a defining feature.

Seizures may be acute symptomatic or unprovoked [19]. The annual incidence of acute symptomatic seizures is 29–39 per 100,000, while the incidence of unprovoked seizures is 23–61 per 100,000 [19]. Regarding mortality, acute symptomatic seizures lack detailed studies, while unprovoked seizures have a standardized mortality ratio (SMR) of 2.3 for single seizures and 2.5–4.1 for newly diagnosed cases [19].

The 2010 classification by the International League Against Epilepsy (ILAE) categorizes seizures into three main types: generalized seizures, focal seizures, and epileptic spasms [63]. Generalized seizures originate in bilateral, widely distributed neuronal networks and include subtypes such as absence seizures, generalized tonic-clonic seizures, myoclonic seizures, and atonic seizures. Focal seizures originate in specific neuronal networks within one cerebral hemisphere, with clinical manifestations depending on the affected brain region. Epileptic spasms are characterized by sudden flexion or extension of extremities held for seconds and recurring in clusters [63].

Studies have identified specific groups of patients at higher risk of seizure recurrence who may benefit significantly from early drug treatment to prevent short-term seizure recurrence [7]. Epilepsy treatment primarily relies on medical therapy, with

most patients achieving good control using a single antiepileptic drug (AED) [42]. However, around 30% of patients with partial epilepsy and 25% with generalized epilepsy do not respond well to AEDs, often requiring multiple drugs, yet still face disabling seizures and significant side effects [42]. For those who do not respond adequately to AEDs, options like surgery and vagus nerve stimulation provide additional therapeutic possibilities [42]. Special considerations are necessary for managing epilepsy in specific populations, such as children, individuals with developmental delays, women, and the elderly, due to their unique needs and challenges [42].

According to [55], the key to the diagnosis of epilepsy is to combine the electrophysiological findings of EEG with clinical seizure symptomatology. The presence of interictal epileptiform discharges (IEDs) supports the diagnosis of epilepsy only if the clinical history provides evidence consistent with one or more previous seizures. The Salzburg Criteria are a standardized process for diagnosing NCSE in the ICU. It deals first with the most clear-cut cases (e.g., firing at frequencies more than 2.5 Hz), then with the less clear-cut cases (e.g., spatiotemporal evolution or clinical correspondence), and finally in the "grey area" using drug testing as a diagnostic basis. Auxiliary imaging: In some cases, functional neuroimaging can assist diagnosis. For example, FDG-PET scan can show focal hypermetabolism in the corresponding brain area during ictal, while SPECT during ictal can show focal hyperperfusion.

1.2 Motivation

My research primarily focuses on detecting seizures from EEG data. This is critical because seizure detection plays a pivotal role in diagnosing epilepsy. For neurobehavioral paroxysmal events, correct diagnosis is the first and most critical step toward effective treatment. An incorrect diagnosis of epilepsy not only subjects patients to unnecessary treatment (such as long-term use of anti-epileptic drugs with side effects) and iatrogenic damage, but more seriously, it delays correct treatment for its true cause (whether it is psychological factors or other physical diseases) [55]. Especially in the intensive care unit (ICU), it is crucial to exclude psychogenic non-epileptic status epilepticus and avoid unnecessary and high-risk aggressive treatments (such as anesthesia and intubation) [26, 49, 50].

In detecting structural lesions in patients with seizures, neuroimaging techniques, particularly MRI, play a critical role and are especially useful for conditions like cortical malformations and hippocampal sclerosis [63]. Advanced imaging modalities, including fMRI, PET, SPECT, and MEG, provide functional and metabolic data to complement structural findings and are primarily used in epilepsy centers for presurgical evaluations. CT remains valuable for detecting acute issues like hemorrhage or tumors, while MRI's superior sensitivity makes it the preferred choice for detailed epilepsy assessments [63].

Metabolic evaluation is crucial for specific syndromes like infantile spasms or neonatal seizures, often involving tests for amino acids, organic acids, and glucose transporter defects to identify metabolic disorders [63]. Genetic testing, including karyotyping, epilepsy gene panels, and whole exome sequencing, plays an increasingly significant role in diagnosing genetic causes of epilepsy [63].

EEG plays a central and indispensable role in the diagnosis and treatment of epilepsy and related diseases, and is the "gold standard" for diagnosis and differential diagnosis. EEG is the most powerful tool for distinguishing epileptic seizures from their many imitators, such as psychogenic seizures, syncope, and metabolic encephalopathy. For latent paroxysmal events in newborns, video-EEG is the only gold standard to determine whether it is epilepsy. It can not only detect latent nonconvulsive epilepsy (NCSE), but also guide treatment and evaluate efficacy, assist positioning and preoperative evaluation, determine prognosis, and provide early warning of complications [55]. For example, after subarachnoid hemorrhage, qEEG changes (such as a decrease in Alpha/Delta ratio) can warn of the occurrence of delayed cerebral ischemia earlier than clinical symptoms or imaging, providing a valuable time window for treatment [8]. Last but not least, EEG is a non-invasive neuroimaging technique used to measure the sum of electrical potentials generated by neuronal populations within the brain [30]. Compared to other neuroimaging techniques, such as functional magnetic resonance imaging (fMRI) and magnetoencephalography (MEG), EEG is both portable and relatively affordable, which enhances its accessibility [30]. However, due to the placement of electrodes on the scalp and the limited number of electrodes, EEG has lower spatial resolution than fMRI. Consequently, EEG primarily captures signals from the brain cortex [30]. Sometimes, EEG may even be more sensitive to subtle changes in brain function than clinical examination. The vast majority of patients with abnormal neurological examinations also have abnormal EEG, but only about 58% of patients with abnormal EEG have clinical abnormalities [54]. Despite its spatial limitations, EEG provides excellent temporal resolution, with the ability to detect changes at the scale of milliseconds [4]. This makes it an ideal tool for capturing the fast dynamics of brain activity.

However, the diagnosis of seizure is always full of challenges. First, scalp EEG has limited sensitivity, and not all epileptic seizures are clearly recorded on scalp EEG. In particular, simple partial seizures originating from a small area of brain tissue or deep brain structures (such as the medial temporal lobe, orbitofrontal lobe) produce weak electrical signals that may not be captured by scalp electrodes. Studies have shown that only about 20%-35% of simple partial seizures can have clear ictal discharges recorded on scalp EEG. In addition, the first routine screening scalp EEG may not reveal clear epileptiform abnormalities in 40%-60% of patients with epilepsy. Seizure mimics and comorbidities can also interfere with disease diagnosis. Frontal lobe epilepsy is the leading imitator of psychogenic non-epileptic seizures (PNES), and its EEG findings can be very insidious or misleading. Many

non-epileptic events, such as syncope, migraine, sleep disorders, and mental disorders, can clinically resemble epileptic seizures and require EEG for identification. About 10% of PNES patients also suffer from epilepsy, which poses a huge challenge to differential diagnosis. The clinical significance of some EEG patterns (e.g., PLEDs, GPDs) is controversial. They are neither entirely ictal nor normal interictal, and interpreting these "gray zone" patterns is extremely challenging [55]. Locating the seizure period in EEG recordings manually is difficult and time consuming; one often needs to skim through tens or even hundreds of hours of EEG recordings. Therefore, automatic detection of seizure activity is of great importance [1]. Compared with manual analysis, automated analysis of EEG signals can convert experts' subjective visual assessment of waveforms into objective, quantifiable mathematical indicators (such as power, entropy, connectivity, etc.), so that EEG features can be accurately measured and compared, providing a solid quantitative foundation for scientific research and clinical diagnosis. It can also screen massive data 24 hours a day, 7 days a week, and mark suspicious events, greatly shortening image reading time and reducing missed reports, improving efficiency and sensitivity. In addition, a large number of epileptic seizures are subclinical, without any external clinical manifestations, or the patients are unable to report them due to ictal amnesia. Automated monitoring is the only reliable means of accurately quantifying the burden of this type of attack. Automated methods can also efficiently reduce data dimensionality and extract features. It can compress a complex EEG waveform containing thousands of data points into a few or dozens of digital features with clear meaning to form a "feature vector", which greatly simplifies the data and facilitates subsequent classification and statistical analysis [55].

Classic automatic detection algorithms include steps such as feature extraction and classification. Feature extraction quantitatively describes each candidate epileptic seizure event, captures its core content, and constructs a "feature vector." It is divided into three basic perspectives: time domain analysis, frequency domain analysis and time-frequency domain analysis. Time domain analysis includes calculating statistics such as mean, variance, skewness, and kurtosis, describing the distribution characteristics of signal amplitude, using autocorrelation to measure the time dependence, internal rhythm, and "memory" of the signal, and using entropy and information measures to quantify the complexity, uncertainty, or "chaos" of the signal, which is often used to evaluate the depth of anesthesia and impairment of consciousness. Frequency Domain Analysis uses Fast Fourier Transform (FFT) to analyze the frequency composition of the signal to obtain the power spectrum. However, reliable spectral estimates must be obtained by period averaging or frequency smoothing. Time-Frequency Analysis combines the time domain and the frequency domain, using a powerful tool such as Wavelet Transform, which can provide "zoom" analysis, using high time resolution for high frequencies and high frequency resolution for low frequencies, which is very suitable for non-stationary EEG signals [55].

The purpose of classification is to assign a final category label (such as "spike", "artifact", etc.) to the event based on the extracted feature vector. It is divided into two categories: supervised classification (Supervised Classification) and unsupervised classification (Unsupervised Classification). The former requires a training data set pre-labeled by experts. The algorithm learns rules from "standard answers". Common classifiers include: Linear classifiers such as Linear Discriminant Analysis (LDA) and Support Vector Machines (SVM), Neural Networks that can learn complex nonlinear relationships, Nonlinear Bayesian Classifiers that classify based on probability, and Nearest Neighbor Classifiers that classify based on distances in feature space. Unsupervised Classification, also known as clustering, does not require any prior labels. The algorithm automatically divides the data into several clusters based only on the similarity of the data itself [55].

Traditional feature-based methods face three major challenges [22]. First, they are highly sensitive to variations in seizure patterns, as EEG signals are non-stationary, and their statistical properties vary across different patients and even within the same patient over time. Second, EEG data are prone to noise, including muscle activity, eye movements, and environmental interference, which can distort genuine EEG features and significantly reduce detection accuracy. Finally, the scalability of these systems is limited, as most existing approaches are trained on small-scale EEG datasets collected from only a few patients, restricting their practicality and applicability in clinical settings [22].

Deep learning can automatically optimize parameters, reducing the reliance on expert knowledge and making it well-suited for handling complex, high-dimensional data like EEG signals [9]. It excels in handling complex and high-dimensional data, such as images, text, and EEG signals, effectively addressing challenges like low signal-to-noise ratio, non-stationarity, and inter-subject variability in EEG [52]. Deep learning has demonstrated strong adaptability in medical imaging and EEG classification, providing a reliable solution for large-scale interpretation of complex data [9].

Convolutional Neural Networks (CNNs) are widely used in deep learning research and were originally designed for image processing [15], and then successfully applied to medical image analysis, [5, 27, 69], remote sensing [20, 34], etc. Recently, they have been adapted into one-dimensional (1D) and two-dimensional (2D) architectures for analyzing biological signals like EEGs, particularly for detecting epileptic seizures [13]. In 2D-CNNs, EEG signals are transformed into 2D representations (e.g., spectrograms, bispectra, wavelet transforms) and used as input [38, 48, 77]. In contrast, 1D-CNNs directly process raw EEG signals, using modified architectures to handle 1D data effectively. Both types are employed for seizure detection and studied for their specific advantages.

Recurrent Neural Networks (RNNs) address challenges associated with sequential data, such as EEG signals, which often have variable lengths and complexity, making it difficult for simpler deep learning methods to process [16].

Autoencoders (AEs) are unsupervised models that compress input data into latent representations and then reconstruct the output, making them ideal for feature extraction and dimensionality reduction in brain signal processing [15, 60, 62, 78]. Restricted Boltzmann Machines (RBMs), foundational to Deep Belief Networks (DBNs), are probabilistic models that learn hierarchical representations of data [15]. DBNs, including variations like Convolutional DBNs (CDBNs), have been used in EEG studies to detect epileptic spikes with high accuracy, as demonstrated by Xuyen et al. [75] and Turner et al. [70].

Despite numerous advantages it has, deep learning method is never a panacea. First of all, it requires a large amount training data and decent calculation resources. Large scale medical data acquisition is always difficult due to privacy and ethical issues. Secondly, deep learning models are often considered "black boxes" because their decision-making processes are not easily interpretable, which can be a significant drawback in clinical settings where understanding the rationale behind decisions is crucial, thus is prone to be rejected by clinical doctors. Lastly, deep learning models can be prone to overfitting, especially when trained on small datasets, leading to poor generalization to new, unseen data. In [55], the authors warn that the performance of automated algorithms (especially supervised learning) depends on the quality of the training data, i.e. the "gold standard" or ground truth. However, in the field of EEG interpretation, there is inherent disagreement among experts, which becomes the most fundamental obstacle to full automation. Automated algorithms will still not be able to completely replace the role of human experts in the foreseeable future.

1.3 Objectives

The primary objective of this research thesis is to develop a robust framework for accurate seizure detection by modeling high-dimensional EEG signals from a graph perspective and enhancing this model with wavelet tools to capture the complex dependencies inherent in EEG data. To achieve this, we focus on two specific research goals.

The first specific objective is to incorporate advanced time-frequency domain features into the analysis of scalp EEG signals. This involves leveraging wavelet methods to perform time-frequency domain analysis across the channels distributed on the scalp, as well as exploring cross-frequency coupling (CFC) to capture the intricate interactions between different frequency bands.

The second specific objective centers on the optimization of Graph Neural Network (GNN) architectures suitable for seizure detection. This entails a comparative analysis of common spectral GNN architectures, including Graph Convolutional Networks (GCN), Spectral Temporal Graph Neural Networks (StemGNN), and Graph Wavelet Neural Networks (GWNN). Furthermore, the research aims to introduce specific modifications to the selected GNN architecture to enhance its

performance in capturing the spatial-temporal dynamics of seizures.

1.4 Structure of the Dissertation

The remainder of this dissertation is organized as follows. Chapter 2 provides a comprehensive overview of existing research on EEG-based seizure detection, ranging from traditional automatic approaches to state-of-the-art methods such as CNN-based and RNN-based models. It places a particular focus on graph-based approaches and time-frequency domain analysis, highlighting the gaps in current methods to establish the need for the proposed framework.

Chapter 3 describes the open-access datasets used in this research, detailing the specific version, structure, and statistical characteristics of the data to ensure reproducibility and clarity regarding the experimental foundation.

Moving to the analytical component, Chapter 4 utilizes time-frequency wavelet tools to characterize within-frequency and cross-frequency functional connectivity during the development of a seizure. It exhibits the statistical significance of these features and reveals their potential utility for downstream machine-learning tasks.

Chapter 5 shifts the focus from the fine-grained dynamical analysis in Chapter 4 to the construction of an efficient, automated detection framework. While Chapter 4 leverages time-frequency tools to dissect the non-stationary evolution of seizures, Chapter 5 aims to develop a Graph Neural Network (GNN) model for binary classification. To achieve computational efficiency and model scalability, this chapter adopts a quasi-stationary assumption over short time windows. This allows us to utilize the Fast Fourier Transform (FFT) to extract robust spectral energy features, which serve as compact node attributes for the GNN to learn complex spatial dependencies.

Finally, Chapter 6 summarizes the contributions made in this thesis, discusses the limitations of the current work, and points out promising directions for future research.

Chapter 2

Literature Review

2.1 Background

2.1.1 Electroencephalography (EEG)

Electroencephalography (EEG) is a medical imaging technique that records electrical activity on the scalp generated by the brain. The EEG signals reflect Local Field Potentials (LFPs), which are fundamentally based on ionic currents flowing through brain tissue [55]. At the cellular level, ionic currents are mainly generated by neurons; glial cells may also be involved [55]. Although Action Potentials (APs) are core signals, their direct contribution to far-field EEG is relatively small due to their short duration and small spatial extent. Postsynaptic Potentials (PSPs) are the primary source of the EEG signal. They are generated when neurotransmitters act on the postsynaptic membrane, changing the permeability of ion channels. PSPs are divided into two types: Excitatory Postsynaptic Potentials (EPSPs) and Inhibitory Postsynaptic Potentials (IPSPs). Specifically, EPSPs cause membrane depolarization, forming an active sink extracellularly (positive ions flow in, making the local area negative). Conversely, IPSPs cause negative ions to flow in or positive ions to flow out, making the local area positive and forming an active source. The extracellular "source" and "sink" generate compensatory ohmic currents, forming current dipoles (a positive pole and a negative pole) [55]. For scalp EEG, these Local Field Potentials (LFPs) pass through different tissues, such as the brain, skull, and scalp, before finally being recorded by EEG equipment on the scalp.

Scalp EEG is a completely non-invasive technique that can be repeatedly applied to patients, healthy adults, and children without significant risks or limitations [66]. The "front end" of all EEG recording systems, which is the part in direct contact with the patient, remains essentially analog. Clinical neurophysiological recordings face a challenging noise environment, including environmental noise, physiological noise etc. Most noise can be several orders of magnitude larger than the target signal. For example, 60 Hz power-line noise from the body can be 10,000 times larger than

the EEG signal, and the ECG signal recorded from the head can be 1,000 times larger than a brainstem evoked potential (EP) signal [55]. The sophisticated design of the analog front end makes it possible to obtain interpretable recordings in such an environment [55]. It allows us to actively lower or eliminate various artifacts while faithfully recording the target signals. For scalp EEG, careful skin preparation and the use of electrolytes can lower the impedance at the electrode-skin contact point. Using the most stable and non-polarizable silver-silver chloride (Ag-AgCl) electrodes is also crucial for obtaining ideal recordings [55]. The amplifier amplifies the raw brainwave signals from the microvolt (μV) level to the much stronger volt (V) level. In practice, the vast majority of environmental noise and physiological noise have nearly identical amplitude and phase in adjacent scalp regions. These are known as common-mode signals. The differential amplifier provides a solution to suppress this type of noise [55]. A differential amplifier has two symmetrical inputs and functions by subtracting the total voltage at one input from the total voltage at the other. The "common" noise component is perfectly canceled out, leaving only the "difference" between the two points—the differential signal that we actually want to measure. Finally, analog filters serve to screen the signal based on frequency [55].

The development of digital analysis and digital storage has revolutionized EEG technology, as its back end processing is now digitized [55]. The fundamental principle of digital EEG is the conversion of a continuous analog signal into discrete numerical values [55]. The component that performs this function is called an analog-to-digital converter (ADC). The output of each analog amplifier is fed into a separate ADC, which transforms the continuous analog signal into a series of discrete binary numbers [55]. Therefore, a set of raw, independent data streams, each recorded relative to a reference electrode are stored. This allows for the flexible reconstruction of a montage as needed for analysis. A montage defines the voltage difference displayed on each channel between two selected electrodes. This includes Bipolar Montages, which link adjacent electrodes in a chain, and Referential Montages, which compare all scalp electrodes to one or more common reference points with theoretically little electrical activity (such as the ear electrodes, A1/A2) etc. These provide different perspectives for analyzing EEG signals [55].

2.1.2 Wavelet Analysis

Traditional Fourier analysis, specifically the Fast Fourier Transform (FFT), is a "descriptive" method that identifies the frequency components composing a signal. However, Fourier transform-based methods rely on the critical assumption of stationarity, implying that the statistical properties of the signal do not change over time. This assumption is often violated in EEG signals, which are inherently non-stationary and exhibit time-varying characteristics, particularly when the research objective is to detect transient events like epileptic seizures. Furthermore,

the seizures themselves are dynamic and constantly evolving processes. To address this limitation, time-frequency analysis methods, such as wavelet transforms, have been developed. The emergence of the wavelet transform represents a major breakthrough in signal processing, especially for non-stationary signals like EEG. It overcomes the inherent limitation of the traditional Fourier transform, which cannot provide simultaneous time and frequency localization, offering a powerful mathematical tool for capturing transient events such as epileptic seizures [67]. Wavelet transforms provide a multi-resolution analysis of signals, enabling the simultaneous capture of both frequency and temporal information. This makes them particularly well-suited for analyzing EEG signals, which often contain transient events that are poorly represented in the frequency domain alone [55]. Additionally, Cross-Wavelet Transform and Wavelet Bispectrum serve as the time-frequency counterparts to Cross-Spectrum and Bispectrum, designed to capture the functional or effective connectivity of EEG signals within or across frequency bands.

Mathematical Formula and Derivation

The Continuous Wavelet Transform (CWT) achieves translation and scaling by computing the inner product of the signal to be analyzed, $x(t)$, with a function known as the "mother wavelet," $\psi(t)$. The mathematical definition is given by:

$$W(s,\tau) = \int_{-\infty}^{\infty} x(t)\psi^*_{s,\tau}(t)dt \tag{2.1}$$

Here, $\psi^*_{s,\tau}(t)$ denotes the complex conjugate of the scaled and translated mother wavelet, defined as:

$$\psi_{s,\tau}(t) = \frac{1}{\sqrt{s}}\psi\left(\frac{t-\tau}{s}\right) \tag{2.2}$$

The parameters in these equations hold distinct physical meanings:

- s is the *scale factor*, which is inversely proportional to frequency. A large scale corresponds to low-frequency information (global view), while a small scale corresponds to high-frequency information (detailed view).
- τ is the *translation factor*, indicating the position in the time domain, allowing the wavelet to shift along the signal.
- $\frac{1}{\sqrt{s}}$ serves as the *energy normalization factor*, ensuring that the energy of the wavelet function remains constant across different scales.
- $*$ indicates the complex conjugate operation.

2.1.3 Cross-Frequency Coupling

Cross-frequency coupling (CFC) is defined as the statistical interaction between neural oscillations of different frequencies, a phenomenon that reflects a higher-order structure in brain activity [40]. It is not simply noise, but a core element of neuronal computation, inter-regional communication, and information processing [76]. CFC mainly includes the following subtypes [2]:

- **Phase-Amplitude Coupling (PAC):** This is the most widely studied form, in which the phase of a low-frequency oscillation modulates the amplitude (or power) of a high-frequency oscillation. This phenomenon is often conceptualized as a process in which local neural processing (high-frequency activity) is nested within and coordinated by large-scale network rhythms (low-frequency phase) [2].
- **Power-to-Power Coupling (PPC) or Amplitude-Amplitude Coupling (AAC):** Refers to the correlation between the power envelopes of two different frequency bands [40].
- **Phase-Phase Coupling or n:m Phase Locking:** Refers to the synchronization between the phases of two oscillations at different frequencies.
- **Phase-Frequency Coupling (PFC):** Refers to the modulation of the frequency of one oscillation by the phase of another oscillation [23].

Researchers have also attempted to elucidate the physiological significance underlying these phenomena. For example, [25] observed that gamma oscillations in the visual cortex are phase-locked with alpha oscillations. This led the authors to hypothesize that gamma oscillations phase-locked to alpha oscillations may facilitate the processing of visual information by temporally segmenting visual representations [55].

2.1.4 Bispectrum

Traditional signal processing methods, such as the Fourier transform, mainly rely on second-order statistics, such as power spectral density. While these methods can effectively reveal the energy distribution of signals at different frequencies, their inherent limitations prevent them from fully capturing all the information contained in complex EEG signals. Furthermore, these second-order methods typically assume that the signal is linear and follows a Gaussian distribution [14, 73].

The neurophysiological basis of seizures involves abnormal, highly synchronized nonlinear interactions within neuronal networks. Therefore, relying solely on the power spectrum leads to the loss of crucial information, particularly the phase coupling relationships between different frequency components. To overcome these limitations, Higher-Order Statistics (HOS) come into play. HOS can

preserve the phase information of the signal and quantify the degree of signal deviation from a Gaussian distribution as well as its nonlinear characteristics, providing a powerful mathematical tool for exploring the neural dynamics underlying EEG signals [14, 73].

Mathematical Formula of the Bispectrum

The bispectrum is strictly defined as the Fourier transform of the third-order cumulant. For a stationary random process $x(t)$, its bispectrum $B(f_1, f_2)$ can be calculated from the expectation of its Fourier transform $X(f)$:

$$B(f_1, f_2) = E[X(f_1)X(f_2)X^*(f_1 + f_2)] \tag{2.3}$$

Here, $E[\cdot]$ represents the expectation operator, and $X^*(f)$ is the complex conjugate of $X(f)$. As can be seen from the formula, the bispectrum is a function of two independent frequencies, f_1 and f_2.

The bispectrum is capable of detecting and quantifying Quadratic Phase Coupling (QPC), which is a form of nonlinear interaction. When two frequency components (e.g., a sinusoidal wave with frequency f_1 and a sinusoidal wave with frequency f_2) interact in a nonlinear system, they generate new frequency components, including the sum frequency ($f_1 + f_2$) and the difference frequency ($|f_1 - f_2|$). If the phase of this newly generated frequency component, $\phi(f_1 + f_2)$, maintains a constant relationship with the sum of the phases of the original frequency components, $\phi(f_1) + \phi(f_2)$, then quadratic phase coupling is said to exist among these three frequency components. A non-zero bispectrum value, $B(f_1, f_2)$, indicates the presence of this phase coupling. For pure linear processes, the bispectrum is theoretically always zero. Therefore, a non-zero bispectrum directly reflects the nonlinearity and non-Gaussian characteristics in the signal, making it an ideal tool for analyzing complex non-stationary signals such as EEG data containing seizure activity.

2.1.5 Graph Signal Processing and Graph Neural Networks

The term “graph signal processing” (GSP) was proposed in seminal works about a decade ago [57, 58, 68, 79]. These works established two complementary theoretical paths: one is a spectral method based on the graph Laplacian matrix, and the other is an algebraic method based on the "shift" operation of the adjacency matrix [33].

Subsequently, these two approaches were unified by a common "graph shift operator" (GSO) framework. Based on this framework, many classic signal processing concepts, such as sampling theory, stationary processes, and filter banks, have been successfully extended to the graph domain. The theory of GSP also provides a solid mathematical foundation for the development of Graph Neural Networks (GNNs), where the convolution operation is rigorously defined as graph filtering [33].

A core application of GSP in neuroscience is to view the brain as a network and brain activity (such as fMRI or EEG signals) as graph signals defined on this network [33]. Researchers use Graph Fourier Transforms (GFTs) to analyze cognitive behavior. For example, studies have found that the energy of high-frequency spectral components in brain signals is related to an individual's ability to switch attention, while the energy distribution across low and high frequencies during learning tasks is related to the familiarity of the task [33]. GSP's advanced tools are also used to reveal localized frequency information in the brain. For example, the multi-resolution properties of the spectral graph wavelet transform are used to capture subtle connectivity patterns in brain activity or to provide biologically meaningful decompositions of fMRI data [33, 46]. GSP can also be used to analyze brain abnormalities or diseases. For instance, comparing energy differences in high- and low-frequency graph spectral components between athletes with multiple concussions and healthy controls can help identify affected brain regions [33, 46].

Spectral GNNs

Deep learning methods utilizing Convolutional Neural Networks (CNNs) and Recurrent Neural Networks (RNNs) have been investigated to address seizure detection challenges. Despite their potential, these architectures fail to capture the spatial relationships between EEG observations across different brain regions, which is a critical factor in understanding the neurological dynamics underlying seizures [17]. Graph Neural Networks (GNNs) offer a novel approach to modeling EEG data, addressing many of these challenges. Unlike traditional deep learning models, GNNs excel at handling graph-structured data. This capability enables GNNs to leverage the spatial-temporal relationships in EEG signals, capturing complex patterns critical for identifying seizures [10, 35, 65].

Spectral GNNs transform graph signals into the frequency domain via the Graph Fourier Transform (GFT), analogous to the Fourier Transform which transforms time-series data into the frequency domain in classical digital signal processing.

First, an eigenvalue decomposition is performed on the graph Laplacian matrix: $\mathbf{L} = \mathbf{U}\mathbf{\Lambda}\mathbf{U}^\top$, where $\mathbf{U}$ is an $N \times N$ orthogonal matrix whose columns constitute the basis of eigenvectors of $\mathbf{L}$, and $\mathbf{\Lambda}$ is a diagonal matrix where the diagonal elements λ_k represent the eigenvalues of $\mathbf{L}$ (graph frequencies).

The GFT of a graph signal (node feature vector) $\mathbf{x} \in \mathbb{R}^N$ is defined as:

$$\hat{\mathbf{x}} = \mathbf{U}^\top \mathbf{x} \tag{2.4}$$

We define the filter as a function $g_\theta(\Lambda)$ that acts on the eigenvalues (frequencies). Mathematically, it is a diagonal matrix where the diagonal elements are $[g_\theta(\Lambda)]_{kk} = g_\theta(\lambda_k)$.

The filtering operation in the spectral domain corresponds to the multiplication

of the matrix and the vector (equivalent to element-wise multiplication):

$$\hat{\mathbf{y}} = g_\theta(\mathbf{\Lambda})\hat{\mathbf{x}} \tag{2.5}$$

Finally, the filtered result $\hat{\mathbf{y}}$ is transformed back to the vertex domain (Inverse GFT):

$$\mathbf{y} = \mathbf{U}\hat{\mathbf{y}} \tag{2.6}$$

By combining the three steps above, we obtain the complete formula for a single graph convolution operation in a spectral GNN:

$$\mathbf{y} = \mathbf{U}g_\theta(\mathbf{\Lambda})\mathbf{U}^\top\mathbf{x} \tag{2.7}$$

Graph wavelets, often utilized within spectral GNN frameworks, successfully extend the powerful multi-resolution and time-frequency localized analysis capabilities of classic wavelets from regular data, such as one-dimensional time signals, to high-dimensional networks [36]. Some works exploit the multi-resolution properties of the spectral graph wavelet transform to capture subtle connectivity patterns in brain activity or provide biologically meaningful decompositions of functional magnetic resonance imaging (fMRI) data [11, 28, 46].

2.2 Related Work

2.2.1 Bispectrum on EEG signals in Seizure Detection

One of the latest advancements in bispectrum research is its application in analyzing effective connectivity to assist in locating the Seizure Onset Zone (SOZ) [14]. In a 2023 study by Gagliano et al. [14], the subjects involved were iEEG recordings from 5 patients with positive postoperative outcomes (i.e., the SOZ was successfully removed). For each seizure, the authors quantified the driving role of each brain region within the epileptic network by calculating the directed reciprocal bispectrum between all pairs of electrode channels, achieving highly convincing results.

Sabor et al. [53] propose employing the wavelet bispectrum to extract features such as phase entropy and normalized bispectral entropy to detect interictal epileptic discharge (IED) events in the open-source scalp EEG dataset from Temple University Hospital. With only 25 significant features, the method achieves a precision of 87.33% and a false-alarm rate of 4.52%.

Ashokkumar et al. [3] extract the mean magnitude, normalized bispectral entropy, and normalized squared entropy of the bispectrum as features of a functional connectivity index (FCI). A graph theory approach is also utilized to analyze brain connectivity patterns for seizure and non-seizure states [3]. This method achieves 99.79%, 100%, and 98.6% in terms of accuracy, specificity, and sensitivity, respectively.

Regarding the limitations of the aforementioned works: [14] focuses on iEEG data, which is invasive and unsuitable for preliminary seizure screening. While [53] facilitates time-frequency analysis with wavelets, it does not study inter-frequency coupling within a more refined scope. A critical limitation is the choice of Discrete Wavelet Transform (DWT) instead of Continuous Wavelet Transform (CWT). Furthermore, it does not utilize graph theory to present the evolution of connectivity across the whole brain during the onset of seizure activity. Although [3] fills the gap in graph analysis, it neglects to utilize wavelet tools and inevitably segments EEG signals into epochs based on a quasi-stationary assumption, which is not always guaranteed. Additionally, it constructs only a single-layer graph, thereby missing the opportunity for inter-frequency coupling graph analysis. Lastly, studying functional connectivity (FC) instead of effective connectivity (EC) limits the ability to provide insights into directional information.

2.2.2 Non-Graph-Based Machine Learning and Deep Learning Methods

Early research in seizure detection primarily relied on traditional machine learning workflows. The core of these methods is manual feature engineering, in which researchers first extract pre-designed features based on specific domain knowledge, such as frequency-domain features, from EEG recordings. These features are then fed into conventional classifiers like K-Nearest Neighbors or Random Forests to identify abnormal EEG signals [37].

The major bottleneck of this approach is its reliance on "manual engineering." The feature extraction process is not only resource- and time-intensive, but the effectiveness of the chosen features directly determines the model's performance, potentially failing to capture all relevant complex patterns in the data.

To overcome the limitations of manual feature engineering, research has gradually shifted towards deep learning models capable of learning features directly from data. Time-series models such as Recurrent Neural Networks (RNNs) have been used to learn directly from raw EEG data, thus eliminating the need for explicit pre-processing steps [51]. Additionally, Autoencoders have been utilized to compress EEG signals into a compact latent space representation to facilitate anomaly detection [59]. Convolutional Neural Networks (CNNs) are among the most widely applied models [61]. A typical strategy involves first converting the one-dimensional signal from each EEG channel into a two-dimensional image format using methods like the wavelet transform, and subsequently applying a CNN for feature extraction and classification [18].

Despite the significant success of these deep learning models, they share a common issue: they often overlook the complex spatial structures of EEG sensors and the geometry of the brain [64]. Whether treating EEG signals as independent time series or as transformed 2D images, these models often fail to effectively capture the physical and spatial relationships between electrodes, which are crucial

for accurate diagnosis.

2.2.3 NeuroGNN

NeuroGNN [17], on which this research is based, introduces a dynamic GNN-based framework designed to construct and analyze graphs that encapsulate the spatial, temporal, semantic, and taxonomic correlations inherent in EEG data. The framework leverages the spatial proximity of electrode placements, temporal dependencies within and across EEG time series, and semantic relationships derived from the neurological functions of the corresponding brain regions. Additionally, it incorporates taxonomic correlations through neuroscientific meta-nodes, extending multi-context modeling to broader brain regions.

Key innovations of NeuroGNN include:

1. **Dynamic Graph Construction:** The framework captures evolving spatial-temporal-semantic correlations by dynamically constructing graphs that reflect the relationships between electrodes and their corresponding brain regions.

2. **Hierarchical Pooling and Meta-Nodes:** Hierarchical pooling is used to handle representations of nodes and meta-nodes, allowing the framework to generalize across broader brain regions.

3. **BiGRUs for Temporal Dependencies:** Bidirectional Gated Recurrent Units (BiGRUs) enhance the model's ability to capture intra-series temporal patterns in EEG data.

4. **Pre-Training for Data Scarcity:** NeuroGNN incorporates a novel pre-training strategy to address the challenge of small training datasets, aligning its learning objective with the graph representation to optimize performance across both detection and classification tasks.

Through extensive experiments with real-world EEG data, NeuroGNN demonstrates state-of-the-art performance, particularly excelling in scenarios involving rare seizure types under data scarcity. Ablation studies confirm the critical contributions of each multi-context correlation modality, highlighting the framework's robustness and adaptability.

2.3 Chapter Summary

In this chapter, we have reviewed the background and related work in the fields of wavelet analysis, cross-frequency coupling, bispectrum analysis, and graph signal processing, as well as their applications in EEG-based seizure detection.

Wavelet analysis is a powerful tool for capturing the time-frequency characteristics of EEG signals, overcoming the limitations of traditional Fourier-based methods. Cross-frequency coupling has been observed, revealing the interactions between different neural oscillations, which is crucial for understanding seizure dynamics. Researchers are also making significant progress in providing physiological interpretations for these phenomena. Bispectrum analysis, as a higher-order statistical method, effectively captures the nonlinear interactions in EEG signals, providing a rigorous mathematical framework for analyzing CFC and other complex dynamics.

Graph signal processing and Graph Neural Networks provide a novel perspective for modeling EEG data, capturing the complex spatial-temporal relationships inherent in brain activity. Spectral GNNs use the Graph Fourier Transform (GFT) to perform convolution operations on graph-structured data, enabling the extraction of meaningful patterns from EEG signal networks.

Finally, the NeuroGNN framework demonstrates state-of-the-art performance in seizure detection tasks. It effectively integrates multi-context correlations and addresses challenges such as data scarcity through innovative pre-training strategies. It defines a pipeline for constructing graphs combining multi-contextual information, aggregating via common GNN algorithms, and pooling to obtain the final classification results.

However, NeuroGNN does not fully explore the impact of different message aggregation architectures and algorithms on the performance of the overall model. Instead, it employs a basic Graph Convolutional Network (GCN) without providing a theoretical justification for this specific choice.

Chapter 3

Data

This chapter introduces and analyzes the dataset used in the thesis.

In this study, we use the Temple University Hospital EEG Seizure Corpus (TUSZ), version 2.0.3 [44, 56], which is one of the world's largest open-access databases for clinical EEG seizure detection and classification research. This corpus is a subset of the TUH EEG Corpus and was specifically developed to support the research and evaluation of machine learning and deep learning-based seizure detection and classification algorithms. TUSZ is a carefully selected and annotated subset of TUEG, aiming at providing a dedicated dataset rich in epileptic events for the development of automatic epilepsy detection and classification technology. In raw clinical EEG data, true epileptic seizure (ictal) events are extremely rare, accounting for less than 0.1% [56]. Therefore, directly performing random sampling on the complete set of TUEG to train an epilepsy detector is extremely inefficient. To address this problem, TUSZ was built using a practical "triage" strategy in order to identify data that are most likely to contain epileptic events from the massive TUEG database. This process combines three methods:

1. Keyword search: Search clinical reports for phrases highly relevant to epileptic seizures, such as "seizure begins with" or "evolution".

2. Commercial software detection: Use industry-leading commercial epilepsy detection software (such as Persyst) to perform preliminary screening of data.

3. Academic research systems: Utilize experimental automated EEG detection systems (such as AutoEEG) for cross-validation [56].

Many files are "pruned" versions of the original clinical records. It is standard clinical practice for clinicians or technicians to delete segments that have no diagnostic significance or are heavily contaminated with artifacts when reviewing the data [56].

All EEG signal data are stored in standard, open European Data Format (.edf) files. EDF files consist of a text header and a binary data part. The header contains

metadata, while the data part contains the continuous sample values of all channels, with varying lengths. This standard format ensures that the data can be easily read and processed by a variety of open-source software.

Physiological artifacts (such as eye movements and muscle activity) and technical artifacts (such as poor electrode contact) in EEG signals constitute one of the main sources of noise in automatic epilepsy detection algorithms. These artifacts are common in TUSZ data. Retaining the original signal characteristics, including noise, was an intentional design choice. This provides the research community with a "raw" dataset close to clinical reality, driving developers to design models that are robust enough to cope with the challenges of real-world signals. This makes TUSZ a challenging and valuable benchmark for clinical prediction.

The dataset is organized into training, development, and evaluation subsets, ensuring proper separation between model development, validation, and blind testing. A total of 7,361 EEG recordings (EDF format) are included, accompanied by event-based and term-based annotations in CSV format. Event-based annotations are provided on a per-channel basis, while bi-class annotations—namely seizure and background—are based on a simplified binary classification scheme.

Some key statistics for the TUH Seizure Corpus v2.0.3 are summarized in Table 3.1.

The EEG signals were processed and analyzed using the standard bipolar Temporal Central Parasagittal (TCP) montage, as defined by the Temple University Hospital (TUH) EEG Corpus framework. Two primary reference schemes were utilized: the Averaged Reference (TCP-AR) and the Linked Ears Reference (TCP-LE). The standard TCP-AR montage consists of 22 channels, while the TCP-LE montage comprises 23 channels, including one for electrocardiogram (EKG) monitoring. These bipolar channels are constructed by differencing signals from pairs of scalp electrodes (e.g., FP1-F7 is derived from EEG FP1-REF − EEG F7-REF).

Event annotation within the dataset follows a comprehensive labeling scheme. Each temporal segment is annotated with labels corresponding to normal background activity (`BCKG`), artifacts, or specific epileptic events. This detailed classification, including subtypes like focal non-specific seizure (`FNSZ`) and tonic-clonic seizure (`TCSZ`), enables a fine-grained analysis of ictal and interictal periods. The definitions for the primary event and seizure labels used in this study are provided in Table 3.2.

The specific definitions for each label presented in Table 3.2 are as follows: BCKG represents baseline or non-interesting neurophysiological events, while SEIZ is a common, general-purpose class that can include all types of seizures. An ABSZ, known as an Absence Seizure (or Petit Mal), is characterized by Absence Discharges on the EEG, during which the patient briefly loses consciousness. A CPSZ is a Complex Partial Seizure, involving partial seizures that occur during a state of unconsciousness, with specific characteristics determined by clinical signs. A FNSZ, or Focal Non-Specific Seizure, indicates a focal seizure that cannot be more

Statistic	Train Set	Dev Set	Eval Set	Total
Files				
.edf files	4664	1832	865	7361
.csv files	-	-	-	7361
.csv_bi files	-	-	-	7361
Sessions				
Total sessions	1175	342	126	1643
Sessions with seizures	352	113	63	528
Patients				
Total patients	579	53	43	675
Patients with seizures	208	45	34	287
Seizure Data				
Files with seizures	872	324	195	1391
Seizure events	2421	1081	469	3971
Duration (seconds)				
Total recordings	3,277,229	1,567,972	459,713	5,304,914
Seizure events	175,125	71,871.8	27,246.7	274,243.5

Table 3.1: Descriptive statistics for the Temple University Hospital Seizure Corpus (TUSZ) v2.0.3.

Class Code	Event Name	Signs	Locality
BCKG	Background	E	All
SEIZ	Seizure	C & E	All
ABSZ	Absence Seizure	C & E	Generalized
CPSZ	Complex Partial Seizure	C & E	All
FNSZ	Focal Non-Specific Seizure	C & E	Hemispheric/Focal
GNSZ	Generalized Non-Specific Seizure	C & E	Generalized
MYSZ	Myoclonic Seizure	C & E	N/A
SPSZ	Simple Partial Seizure	C & E	All
TCSZ	Tonic Clonic Seizure	C & E	All
TNSZ	Tonic Seizure	C & E	All

(E = Electrographic, C = Clinical)

Table 3.2: Definitions of the primary event and seizure type annotations used in the TUH Seizure Corpus.

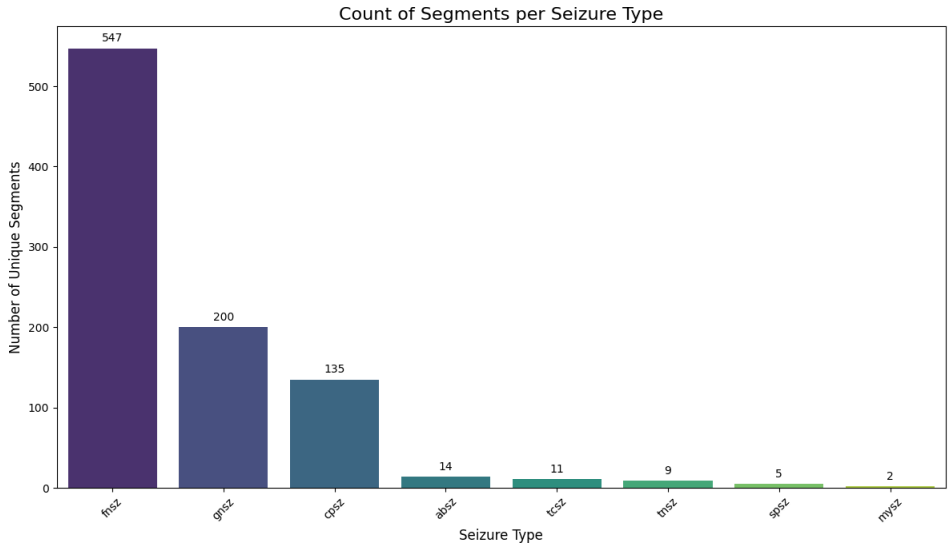

Figure 3.1: Frequency distribution of annotated seizure types within the dataset.

specifically categorized, whereas a GNSZ (Generalized Non-Specific Seizure) refers to generalized seizures that cannot be further classified. A MYSZ is a Myoclonic Seizure, characterized by myoclonic jerks of the limbs, while a SPSZ is a Simple Partial Seizure, which involves partial seizures where the patient remains conscious. Lastly, a TCSZ, or Tonic-Clonic Seizure (Grand Mal), begins with a tonic phase (stiffening of the body) followed by a clonic phase (jerking), and a TNSZ is a Tonic Seizure characterized by the stiffening of the body, during which the ictal EEG patterns may be obscured or disappear.

Below we have detailed statistical information on the training dataset, which will be used in the following chapter and the training phase of subsequent chapters.

First, it is reasonable to examine the distribution of seizure types within the dataset, as shown in Figure 3.1. Each bar represents the total number of unique segments where a specific seizure type was identified, illustrating the significant class imbalance across categories. The figure illustrates the significant class imbalance across different seizure categories, with some types being much more prevalent than others.

In cases where a single segment contained multiple distinct seizure types, the frequency of each combination was tallied, as presented in Table 3.3.

For each seizure type, we also analyzed duration distribution and statistics, providing a fine-grained scope on a seizure type basis. Figures 3.2 through 3.9 present these distributions as histograms. In each figure, the total height of a bar indicates the number of segments within a specific duration bin, while the lower, red portion of the bar illustrates the average proportion of that duration that corresponds to actual seizure activity.

Seizure Combination	Count
`fnsz, gnsz`	48
`cpsz, fnsz`	3

Table 3.3: Frequency of co-occurring seizure type combinations found within a single segment.

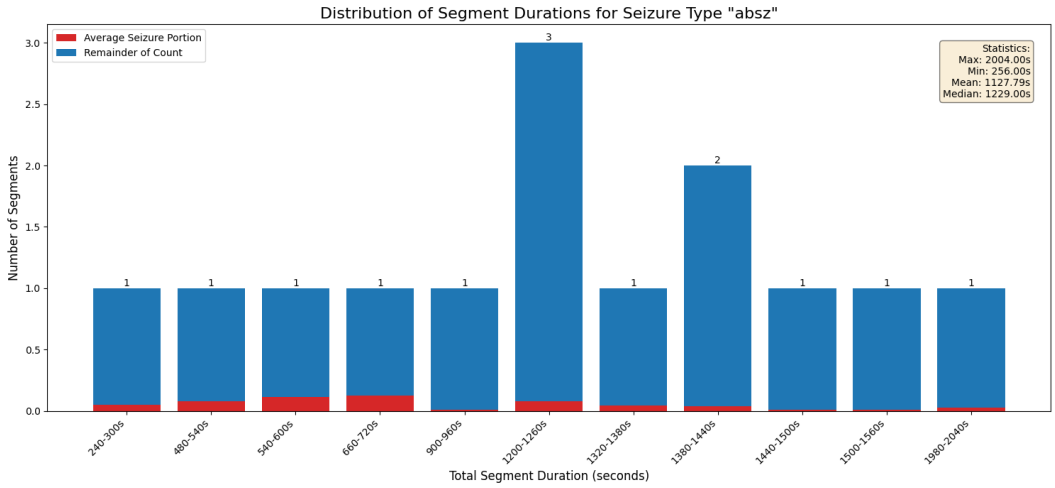

Figure 3.2: Distribution of total segment durations for segments containing the `absz` (Absence Seizure) annotation.

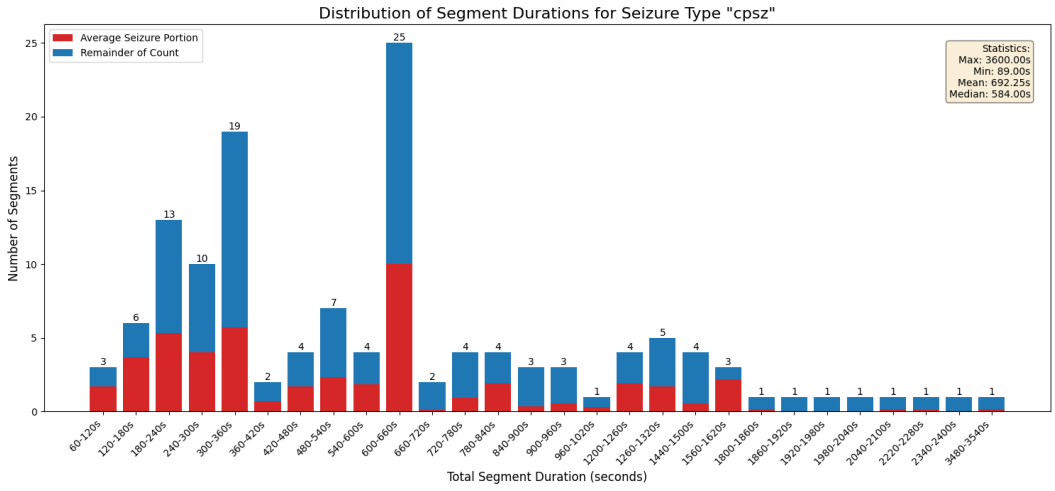

Figure 3.3: Distribution of total segment durations for segments containing the `cpsz` (Complex Partial Seizure) annotation.

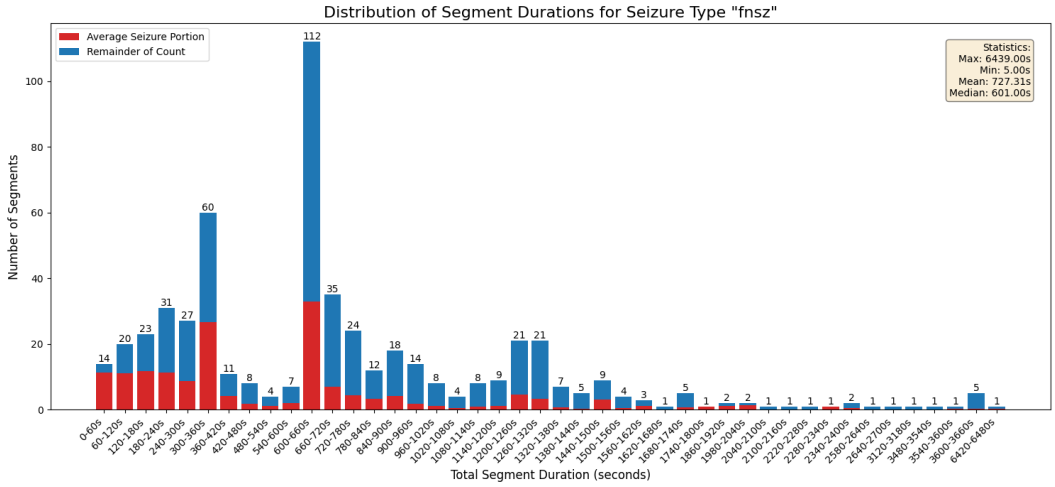

Figure 3.4: Distribution of total segment durations for segments containing the `fnsz` (Focal Non-Specific Seizure) annotation.

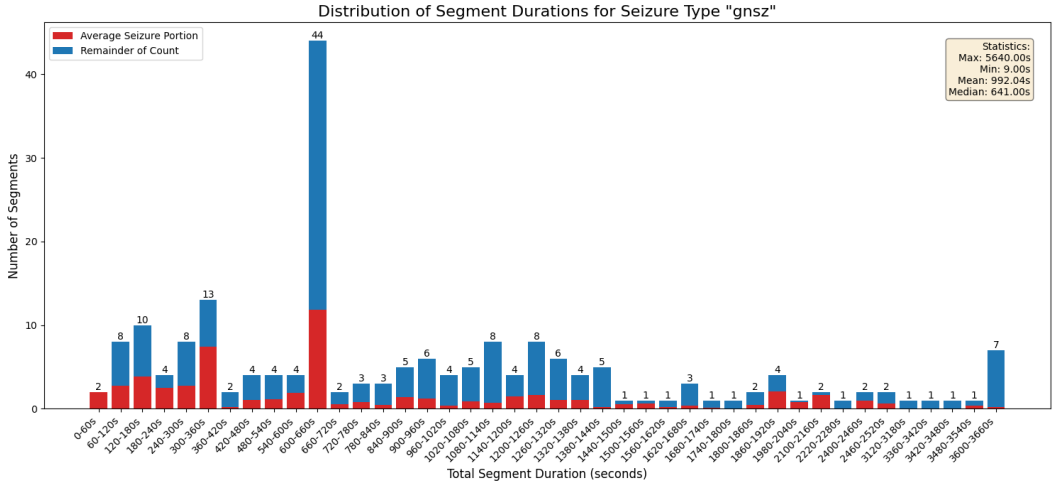

Figure 3.5: Distribution of total segment durations for segments containing the `gnsz` (Generalized Non-Specific Seizure) annotation.

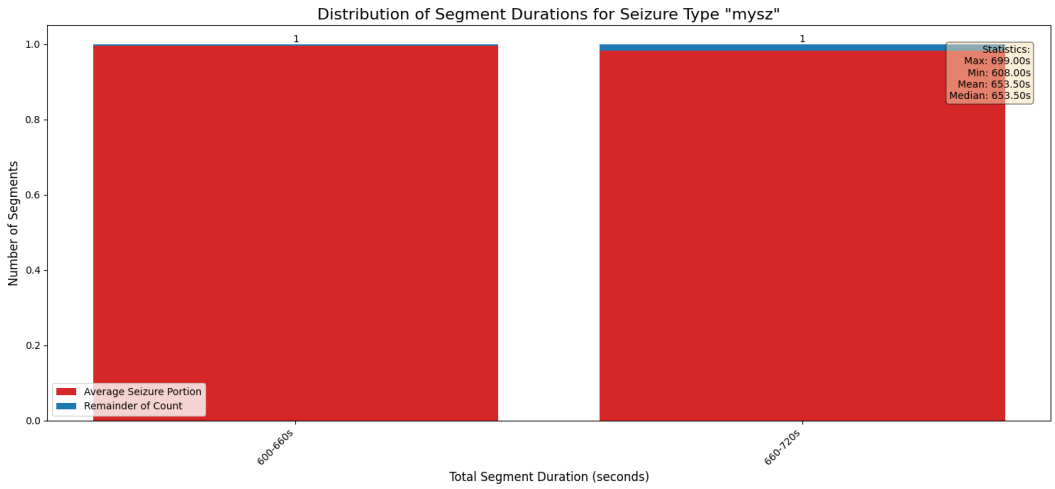

Figure 3.6: Distribution of total segment durations for segments containing the `mysz` (Myoclonic Seizure) annotation.

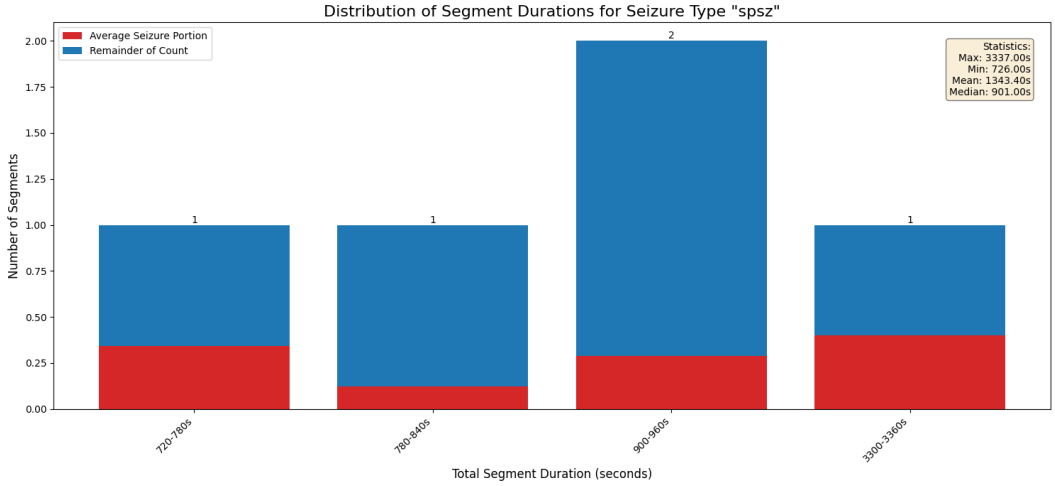

Figure 3.7: Distribution of total segment durations for segments containing the `spsz` (Simple Partial Seizure) annotation.

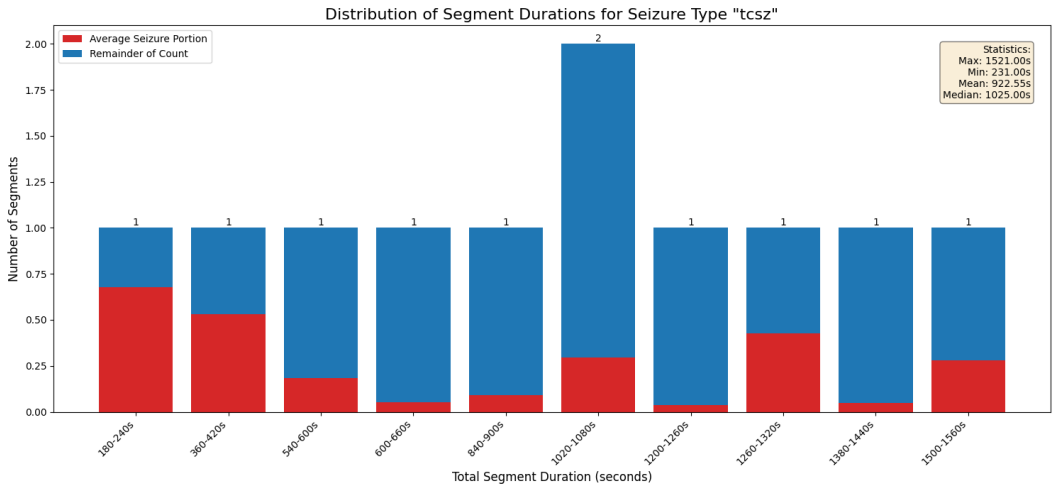

Figure 3.8: Distribution of total segment durations for segments containing the `tcsz` (Tonic Clonic Seizure) annotation.

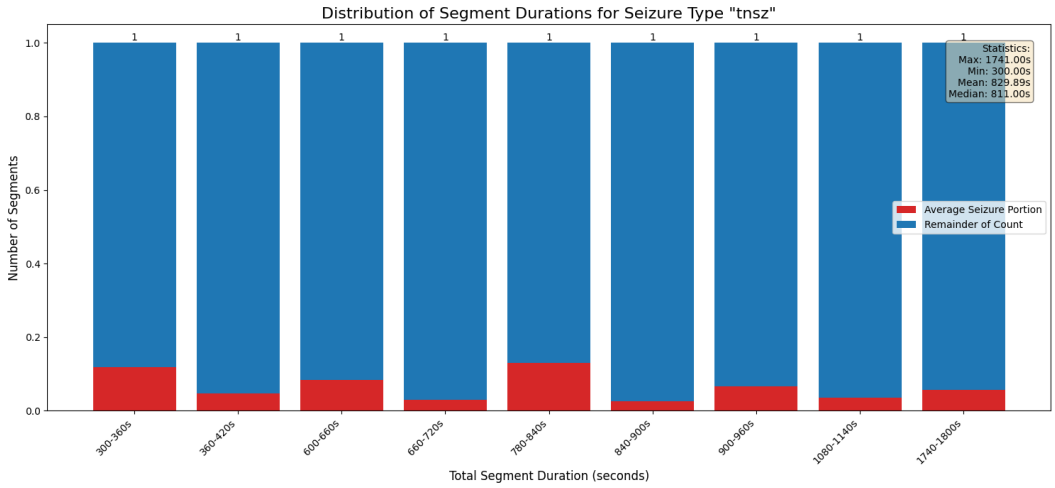

Figure 3.9: Distribution of total segment durations for segments containing the `tnsz` (Tonic Seizure) annotation.

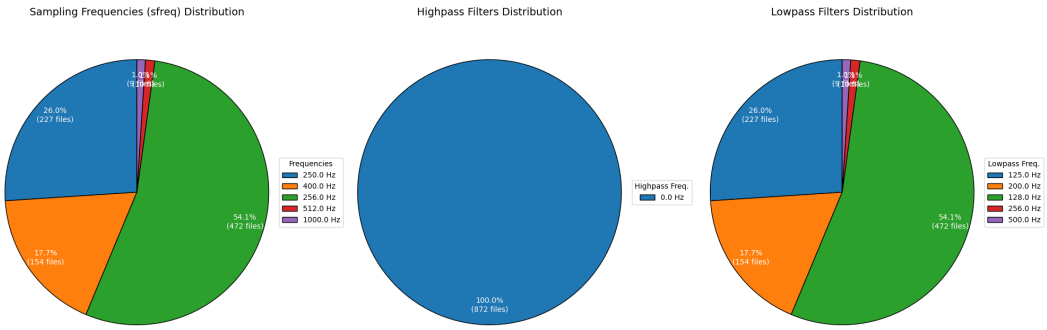

Figure 3.10: Distribution of key technical parameters across the dataset files.

Finally, the following pie chart, Figure 3.10, provides a technical note on the statistics regarding sampling frequencies, high-pass, and low-pass configurations, which are significant for the frequency analysis in the following chapters. The charts show the proportion of files recorded with different (a) sampling frequencies (*sfreq*), (b) high-pass filter cutoffs, and (c) low-pass filter cutoffs. The data demonstrate a variety of sampling frequencies (*sfreq*), with 256.0 Hz being the most predominant (54.1%), followed by 250.0 Hz (26.0%) and 400.0 Hz (17.7%). Notably, a universal high-pass filter setting of 0.0 Hz was observed across all files, suggesting that no high-pass filtering was applied during data acquisition. Correspondingly, the low-pass filter cutoffs align with the sampling frequencies, typically set at or below half the sampling rate to prevent aliasing.

Chapter 4

Cross-Frequency Graph Analysis with Wavelet Bispectrum-based Functional Connectivity

4.1 Introduction

Many seizures are characterized by hyper-synchronization across the brain. For example, the typical characteristic of ictal EEG in childhood absence epilepsy (CAE) is symmetrical spike-and-wave discharges with a frequency higher than 2.5 Hz throughout the brain [47, 55]. The terms “symmetry” and “whole brain” here reflect the concept of high synchronization. In continuous spike-waves during slow sleep (CSWS), immediately after entering non-rapid eye movement sleep, the EEG is "submerged" by persistent, bilateral diffuse spikes and waves [55]. "Bilateral diffuse" also refers to a wide range of synchronized discharges across hemispheres.

From a signal processing perspective, we can use Functional Connectivity (FC) to describe the statistical dependence (i.e., "synchronicity") between signals in different areas of the brain, and Effective Connectivity (EC) to describe the directed and causal influence of one brain area on another [55]. Wendling et al. [72] utilized intracranial EEG and nonlinear correlation rate (h^2) metrics to quantify the dynamic changes in brain networks during seizures. Research has found that at the moment of seizure onset, synchrony (h^2 value) within the limbic system sharply increases, and as the seizure progresses, this highly synchronized state spreads from the limbic system to other brain areas [72]. However, these studies fail to integrate cross-frequency coupling (CFC) information. By leveraging bispectrum analysis, some recent studies have revealed nonlinear interactions in the brain during seizures, successfully facilitating seizure prediction or even the localization of the Seizure Onset Zone (SOZ) [14].

Nevertheless, the aforementioned research on the bispectrum treats EEG signals as stationary. This assumption is problematic for non-stationary EEG signals whose frequency content changes drastically over time, especially during seizure state transitions. For example, a normal background rhythm may suddenly be replaced by high-frequency, high-amplitude epileptiform discharges. The Fourier transform and traditional bispectrum can only indicate that these frequency components "exist," but they cannot specify "when" they appear. Consequently, research is often forced to divide signals into segments and proceed under the assumption that they are locally stationary. The length of these segments is often decided empirically.

In order to simultaneously capture the precise time and frequency domain characteristics of a signal, time-frequency analysis methods must be used, and the wavelet transform is one of the most powerful and flexible tools available. This chapter aims to upgrade the current methodology to a dynamic version in the time-frequency domain, which is exempt from the quasi-stationary assumption, thereby eliminating the need for segmentation. Additionally, this is the first study attempting to use scalp EEG signals for this purpose, whereas prior works have focused on iEEG datasets.

4.2 Proposed Method

4.2.1 Cross Wavelet Transform (XWT)

For two time series, x_n and y_n, with their respective Continuous Wavelet Transforms (CWTs) being $W_n^X(s)$ and $W_n^Y(s)$, the Cross-Wavelet Spectrum, $W_n^{XY}(s)$, is defined as:

$$W_n^{XY}(s) = W_n^X(s)W_n^{Y*}(s)$$

The Cross-Wavelet Spectrum $W_n^{XY}(s)$ is a complex value that quantifies the local covariance between X and Y in the time-frequency space. $|W_n^{XY}(s)|$ represents the cross-wavelet power, which is the power shared by the two signals, reflecting the intensity of their common variation.

4.2.2 Wavelet Bispectrum (WB)

Although XWT performs localized analysis of linear correlation based on second-order statistics (cophase and power), many biological signals, especially EEG signals in pathological states, exhibit significant nonlinear responses. Key features of these dynamics, such as Phase-Amplitude Coupling (PAC), cannot be detected by second-order methods alone. Therefore, Higher-Order Spectral analysis (HOS), such as the bispectrum, is needed to capture these nonlinear characteristics [43].

Traditional power spectra completely discard phase information, making them unable to distinguish signals that have the same power spectrum but different

waveforms. In contrast, HOS methods like the third-order bispectrum preserve phase information, thereby enabling the detection of nonlinearity and non-Gaussian characteristics. The bispectrum is particularly useful for quantifying *Quadratic Phase Coupling* (QPC). When oscillations at two frequencies, f_1 and f_2, pass through a nonlinear system, they can generate a new frequency component with frequency $f_1 + f_2$ and phase $\phi_1 + \phi_2$. The bispectrum can detect this specific phase relationship, whereas the power spectrum cannot. In neural signals, the presence of QPC may indicate nonlinear interactions between different neural ensembles.

To capture these dynamics over time, we extend this concept to the Wavelet Bispectrum (WB) by substituting the Fourier transform with the wavelet transform. A more rigorous definition comes from [43]:

$$b_{\psi,\kappa,xyz}(f_1, f_2, t) = D_\psi(\langle f_1, f_2 \rangle)^{-1} W_{\psi,\kappa,x}(f_1, t) W_{\psi,\kappa,y}(f_2, t) W^*_{\psi,\kappa,z}(f_1 + f_2, t) \quad (4.1)$$

where $W_{\psi,\kappa,x}(f, t)$ is the wavelet transform of signal x at frequency f and time t, and $D_\psi(\cdot)$ is a normalization factor based on the mother wavelet ψ, used to normalize the contribution from different frequency combinations.

The core idea of this formula is as follows: at time point t, the wavelet coefficients at frequencies f_1 and f_2 are multiplied, and this product is then multiplied by the complex conjugate of the wavelet coefficient at the sum frequency $f_1 + f_2$. If QPC exists, the phase of this product will cancel out, and after averaging over many instances, a large magnitude will be obtained. Following the method in [31], we set $y = z$, and use the absolute value $|b_{\psi,\kappa,xyy}(f_1, f_2, t)|$ to quantify the strength of CFC from signal x at frequency f_1 to signal y at frequency f_2 at time t.

4.2.3 Network Measures

Single Layer Network Measures for XWT

We build a network for each patient, with each node representing an EEG channel. The edge weight between nodes is defined as the average cross-wavelet power within specific frequency bands (delta, theta, alpha, beta, gamma) over the entire seizure or non-seizure period. To bridge the gap between graph topology and clinical interpretation, we compute the following network measures and discuss their physiological implications:

Node Strength. The node strength is calculated as:

$$s_i = \sum_{j \in N} w_{ij} \quad (4.2)$$

where s_i is the strength of node i, w_{ij} is the weight of the edge between nodes i and j, and N is the set of all nodes in the network. In terms of its clinical significance, node strength reflects the overall connectivity of a node within the network. In the

context of epilepsy, nodes with high strength often act as "hubs" of pathological activity. An abnormal increase in node strength typically indicates the recruitment of that brain region into the seizure network, making it a potential candidate for the Seizure Onset Zone (SOZ) or a primary propagation pathway.

Clustering Coefficient. The clustering coefficient is defined as:

$$C_i = \frac{1}{k_i(k_i - 1)} \sum_{j,h} (w_{ij} w_{ih} w_{jh})^{1/3} \tag{4.3}$$

where C_i is the clustering coefficient of node i, k_i is the degree of node i, and w_{ij}, w_{ih}, and w_{jh} are the weights of the edges connecting nodes i, j, and h. In terms of its clinical significance, the clustering coefficient measures the tendency of nodes to form tightly connected groups. A high clustering coefficient implies strong local integration. In focal seizures, this metric helps characterize the localized hypersynchronization within the epileptogenic zone before the seizure generalizes to the rest of the brain.

Minimum Spanning Tree (MST). The MST weight is computed as:

$$L = \sum_{(i,j) \in MST} w_{ij} \tag{4.4}$$

where L is the total weight of the MST, and w_{ij} is the weight of the edge between nodes i and j in the MST. In terms of its clinical significance, the MST captures the "backbone" of the functional network—the most efficient way to connect all nodes without forming cycles. During seizures, the brain network often shifts towards a more regular and ordered topology. The MST weight and structure allow us to visualize the simplification of brain dynamics during ictal states, reflecting the path of least resistance for seizure propagation.

Maximum Flow. The maximum flow is determined by:

$$F_{max} = \max \sum_{(i,j) \in E} f_{ij} \tag{4.5}$$

where F_{max} is the maximum flow from a source node to a sink node, f_{ij} is the flow through edge (i, j), and E is the set of all edges in the network. In terms of its clinical significance, maximum flow quantifies the maximum amount of information (or in this case, neural signal capacity) that can be transmitted through the network. A higher max flow during a seizure suggests that the pathological network has established a high-capacity infrastructure to sustain and propagate excessive neuronal discharges across brain regions.

Multilayer Network Measures for WB

For the Wavelet Bispectrum (WB) analysis, we construct a multilayer network to capture the complex interplay between different frequency oscillations [31].

Network Construction: The network consists of five distinct layers ($L = 5$), corresponding to the standard EEG frequency bands: Delta, Theta, Alpha, Beta, and Gamma. Nodes within each layer represent the physical scalp electrodes.

- **Intra-layer edges:** Represent connectivity between electrodes within the same frequency band.
- **Inter-layer edges:** Represent the cross-frequency coupling (specifically, the cross-wavelet bispectrum value) between different frequency bands.

This structure allows us to model the brain not as a flat graph, but as a multiplex system where different rhythms interact. To evaluate this structure, we first introduce the concept of Network Efficiency before deriving Vulnerability measures.

Network Efficiency. Network efficiency is a measure of how effectively information is exchanged within the network. It is inversely related to the shortest path length between nodes.

$$E_{global} = \frac{1}{N(N-1)} \sum_{i \neq j \in G} \frac{1}{d_{ij}} \tag{4.6}$$

where N is the number of nodes and d_{ij} is the shortest path length between node i and node j. Similarly, local efficiency (E_{local}) is calculated on the subgraph of neighbors of a node.

Why do we care about efficiency in an EEG model? In the context of a seizure, high Global Efficiency implies that the network is in a "hyper-connected" state, where pathological discharges can rapidly traverse from the focus to remote brain regions. An "efficient" seizure network is, paradoxically, a robust pathological state that is difficult for the brain's inhibition mechanisms to terminate. Understanding efficiency helps us characterize the "speed" and "ease" of seizure propagation.

Global Vulnerability. Global vulnerability is defined as:

$$V = \frac{E_{global} - E_{global}^{removed}}{E_{global}} \tag{4.7}$$

where E_{global} is the global efficiency of the original multilayer network, and $E_{global}^{removed}$ is the global efficiency after removing a specific layer or set of nodes.

Global vulnerability quantifies the fragility of the network structure. It answers the critical clinical question: "If we disrupt a specific connection between two nodes

within a frequency band or across different frequency bands, does the seizure network collapse?" If removing a specific component leads to a high vulnerability score (i.e., a drastic drop in efficiency), that component is a critical "hub" maintaining the seizure. Identifying these high-vulnerability points provides theoretical motivation for therapeutic interventions, such as surgical resection or targeted neuromodulation, aiming to break the efficiency of the seizure network.

Local Vulnerability. Local vulnerability is defined as:

$$V_{local} = \frac{E_{local} - E_{local}^{removed}}{E_{local}} \tag{4.8}$$

where E_{local} is the local efficiency of the original multilayer network, and $E_{local}^{removed}$ is the local efficiency after removing a specific layer or set of nodes.

While global vulnerability assesses the entire brain's susceptibility, local vulnerability measures the resilience of specific local clusters. High local vulnerability in a specific region during the interictal or preictal period may serve as a biomarker for the epileptogenic zone, indicating a region that is structurally crucial for maintaining the local abnormal network even before the seizure generalizes.

4.3 Results & Discussion

4.3.1 XWT-based Analysis

Case Study

Firstly, we applied XWT on the given segment between major pairs of EEG channels across different frequency bands (delta, theta, alpha, beta, gamma). Figure 4.1 shows the cross-wavelet power between all pairs of channels in each frequency band, where the pale red shaded area indicates the seizure period. It can be observed that during the seizure period, there is a significant increase in cross-wavelet power across multiple channel pairs and frequency bands, indicating heightened synchronization and connectivity during the seizure event. This suggests that seizures involve widespread interactions across different brain regions and frequency bands, which can be effectively captured using XWT-based functional connectivity analysis. However, some channel pairs and frequency bands show less significant changes. For example, the Theta band XWT displays consistent power and variance across the entire period, regardless of seizure or non-seizure states. In addition, we notice that the general XWT power level of the Delta band is tenfold higher than that of other bands.

On the channel pair level, there are also distinct patterns. For example, O1-T5, located in the left occipital and left temporal lobes respectively, shows an apparent decrease in XWT power in the Theta band during the seizure period (Figure 4.2),

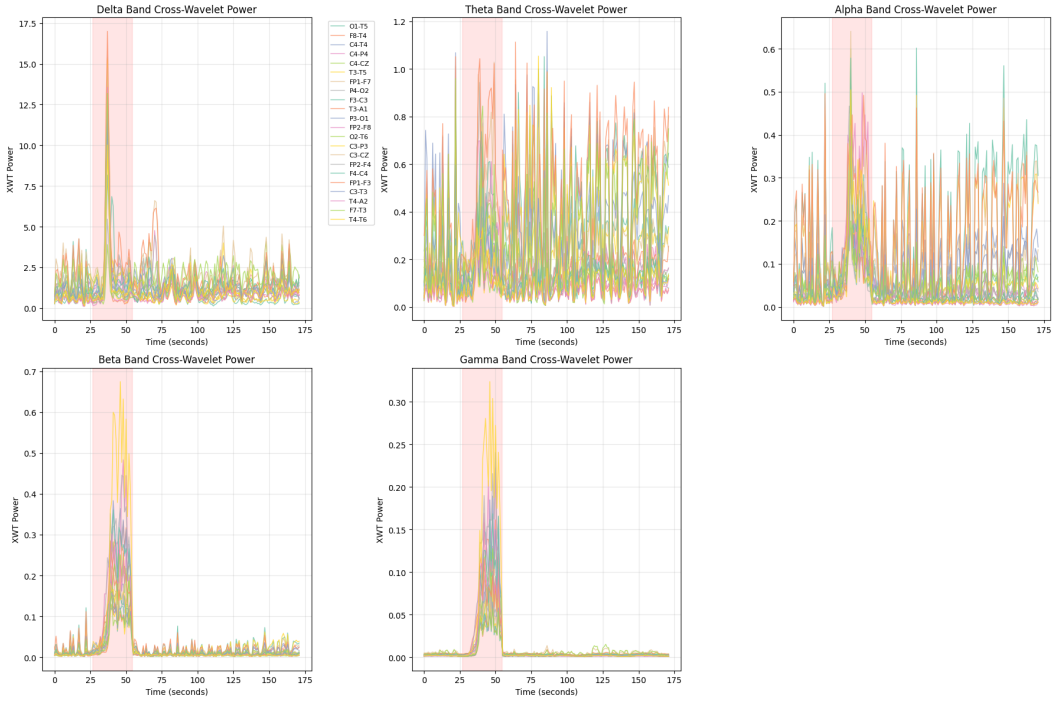

Figure 4.1: Cross-Wavelet Power between all pairs of channels across different frequency bands.

where the pale red shaded area indicates the seizure period. In contrast, F4-C4, located in the right frontal and right central regions, exhibits a significant increase in XWT power in all frequency bands during the seizure (Figure 4.3). However, FP1-F5, located in the left prefrontal and left frontal regions, shows minimal changes in XWT power across the Theta band during the seizure (Figure 4.4). Nearly all channel pairs show a significant increase in XWT power in the Beta and Gamma frequency bands during the seizure period, indicating that high-frequency oscillations play a crucial role in seizure dynamics and brain connectivity changes. This observation aligns with previous findings that high-frequency activity is often associated with seizure events and may contribute to the propagation of seizure activity across brain regions. Additionally, we observe an abrupt, instant increase in Delta band XWT power at seizure onset on all channel pairs, which may reflect the sudden disruption of normal brain activity and the emergence of pathological oscillations during seizure initiation.

Statistical Analysis

Figure 4.5 shows the heatmaps of cross-wavelet power differences between seizure and non-seizure periods across all channel pairs and frequency bands. Red indicates

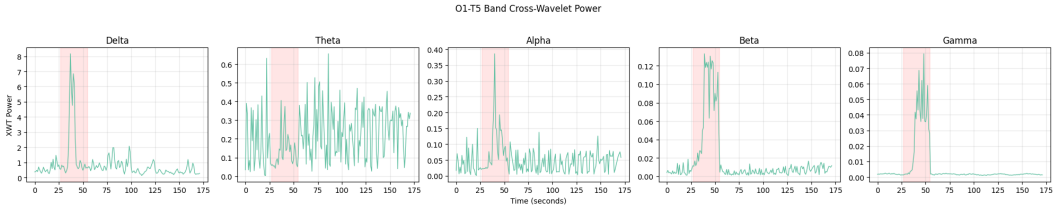

Figure 4.2: Cross-Wavelet Power between O1 and T5 across different frequency bands.

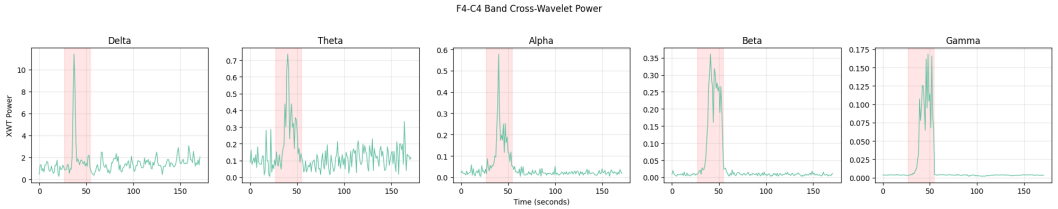

Figure 4.3: Cross-Wavelet Power between F4 and C4 across different frequency bands.

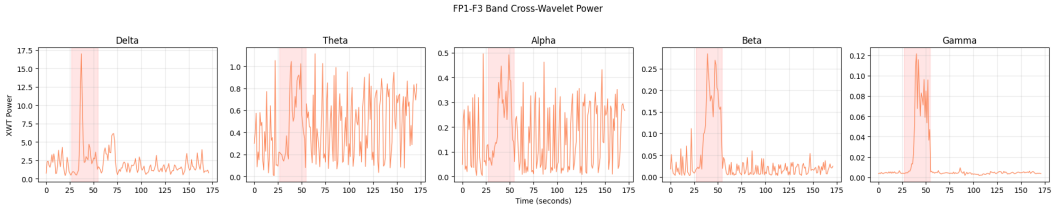

Figure 4.4: Cross-Wavelet Power between FP1 and F5 across different frequency bands.

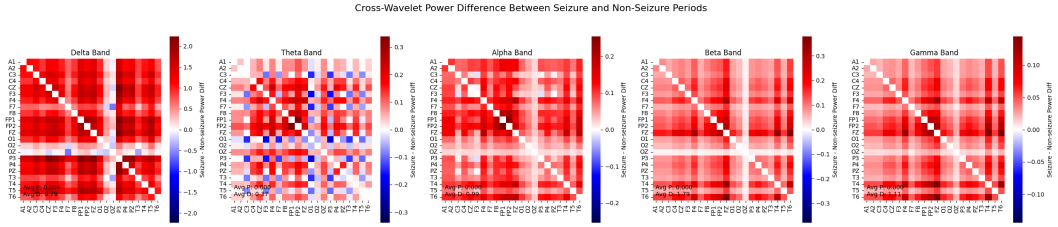

Figure 4.5: Heatmaps of Cross-Wavelet Power differences between seizure and non-seizure periods across all channel pairs and frequency bands.

higher power during seizures, while blue indicates lower power. Each subplot corresponds to a frequency band, with statistical significance and effect size displayed in the bottom left corner. The heatmaps provide a comprehensive overview of how functional connectivity patterns change during seizures across different frequency bands and brain regions. Notably, the Alpha, Beta, and Gamma bands exhibit widespread increases in cross-wavelet power during seizures, as indicated by the predominance of red areas in these subplots. This suggests that high-frequency oscillations play a crucial role in seizure dynamics and brain connectivity changes. The Delta band, however, shows a higher intensity of power differences across most channel pairs while having sporadic pairs with decreases during seizures. The Theta band shows more channel pairs with decreased XWT power during seizures compared to other bands. The statistical significance and effect size values further support the robustness of these findings, indicating that the observed changes in cross-wavelet power are not due to random chance. Overall, these results highlight the utility of XWT-based functional connectivity analysis in capturing the complex dynamics of brain networks during seizure events.

Network Analysis

Figure 4.6, Figure 4.7, and Figure 4.8 show the plots of network measures computed from the XWT-based functional connectivity matrices during seizure and non-seizure periods across different frequency bands. Each subplot corresponds to a specific network measure (Node Strength, Clustering Coefficient, Minimum Spanning Tree, Maximum Flow) and displays the values for seizure (red) and non-seizure (blue) conditions. We can observe that in frequency bands other than Theta, Node Strength (Figure 4.6), MST weight (Figure 4.7, right), and Maximum Flow (Figure 4.8) are significantly higher during seizure periods compared to non-seizure periods. This indicates that during seizures, there is an overall increase in connectivity strength, efficiency of information transfer, and capacity for information flow within the brain network. The Clustering Coefficient (Figure 4.7) also shows a similar trend, with higher values during seizures in most frequency bands, suggesting increased local interconnectedness among brain regions during seizure events. However, the Theta band exhibits a different pattern, with some measures showing less pronounced differences between seizure and non-seizure conditions. This may reflect the unique role of Theta oscillations in brain dynamics during seizures, potentially involving more complex interactions that are not fully captured by these network measures. Overall, these results highlight the utility of XWT-based functional connectivity analysis in revealing the altered network properties associated with seizure activity across different frequency bands. The Average Clustering Coefficient (Figure 4.7, left), however, shows no significant difference in any of the frequency bands.

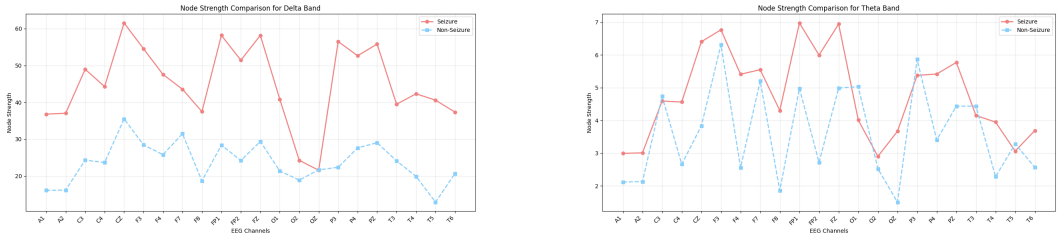

(a) Delta Band (b) Theta Band

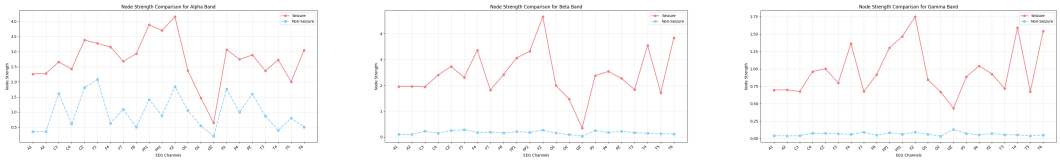

(c) Alpha Band (d) Beta Band (e) Gamma Band

Figure 4.6: Node Strength across different frequency bands during seizure and non-seizure periods.

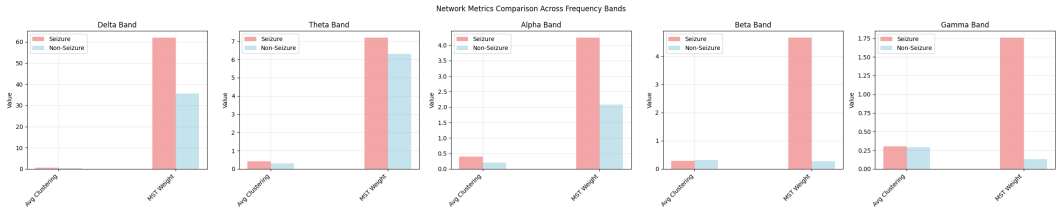

Figure 4.7: Clustering Coefficient and MST weight across different frequency bands during seizure and non-seizure periods.

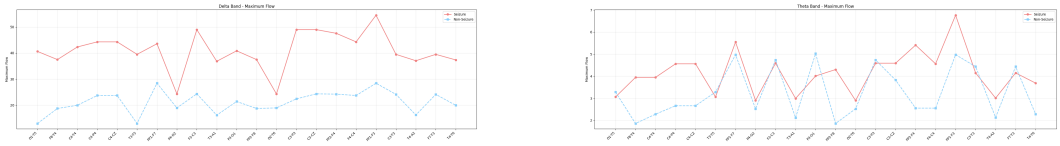

(a) Delta Band (b) Theta Band

(c) Alpha Band (d) Beta Band (e) Gamma Band

Figure 4.8: Maximum Flow across different frequency bands during seizure and non-seizure periods.

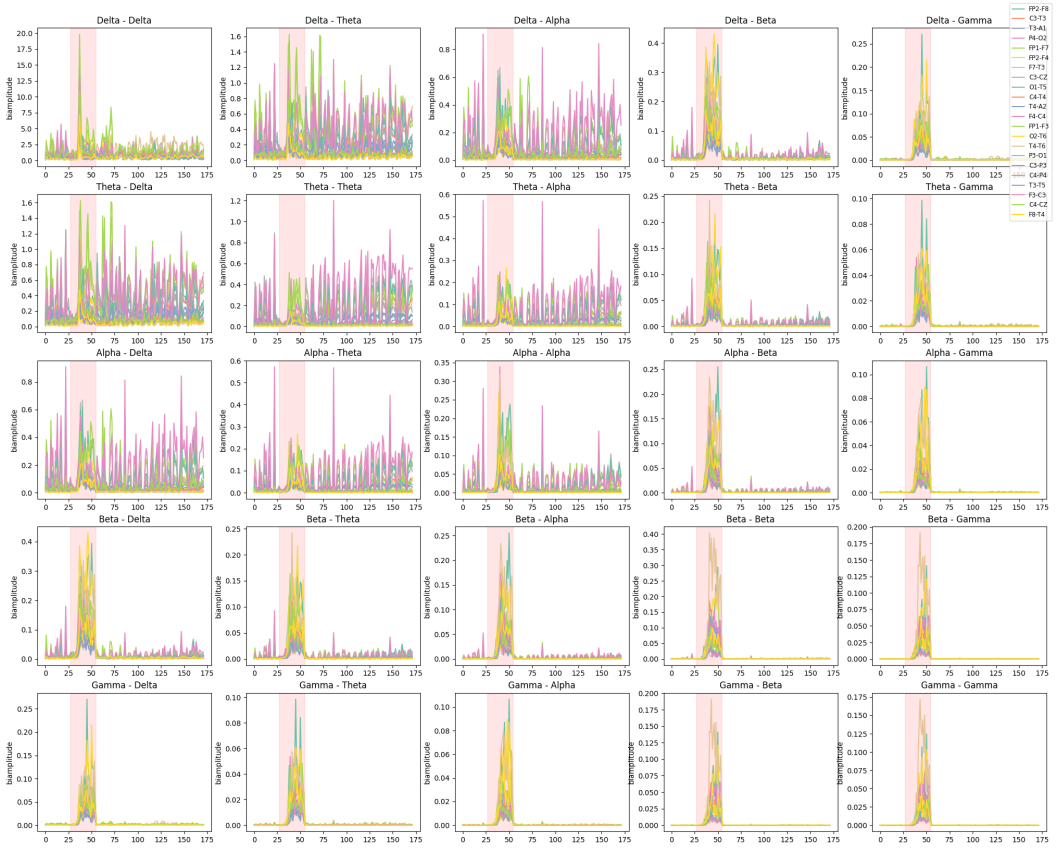

Figure 4.9: Wavelet Biamplitude between all pairs of channels across different frequency band couplings.

4.3.2 WB-based Analysis

Case Study

Similar to XWT, we first applied WB on the given segment between major pairs of EEG channels across different frequency band couplings (e.g., Delta-Delta, Delta-Theta, ..., Gamma-Gamma). Figure 4.9 shows the wavelet biamplitude between all pairs of channels in each frequency band coupling, where We observe that the couplings involving higher frequency bands (Beta and Gamma) exhibit more pronounced changes in biamplitude during the seizure period compared to lower frequency band couplings. However, Delta-Delta coupling shows a significant increase in biamplitude at seizure onset, similar to the XWT results. This suggests that higher frequency oscillations play a crucial role in seizure dynamics and brain connectivity changes, while lower frequency couplings may have more complex interactions during seizures.

Statistical Analysis

Figure 4.10 shows the heatmaps of wavelet biamplitude differences between seizure and non-seizure periods across all channel pairs and frequency band couplings. Red indicates higher values during seizures, while blue indicates lower values. Each subplot corresponds to a frequency band coupling, with statistical significance and effect size displayed in the bottom left corner. The heatmaps provide a comprehensive overview of how cross-frequency coupling patterns change during seizures across different brain regions.

In terms of biamplitude (Figure 4.10), couplings involving higher frequency bands (Beta and Gamma) exhibit more consistent increased values during seizures, and Delta-Delta shows stable negative coupling, while others show scattered decreases. However, the absolute values of higher frequency couplings are generally lower than those of lower frequency couplings, indicating that while higher frequency interactions are more consistently elevated during seizures, their overall strength may be weaker compared to lower frequency interactions. The statistical significance and effect size values further support the robustness of these findings, indicating that the observed changes in wavelet biamplitude are not due to random chance. Overall, these results highlight the utility of WB-based cross-frequency coupling analysis in capturing the complex dynamics of brain networks during seizure events.

Multilayer Network Analysis

Case Study: Figure 4.11 and Figure 4.12 show the plots of multilayer network measures computed from the WB-based cross-frequency coupling matrices in terms of biamplitude during seizure and non-seizure periods across different frequency band couplings. Here, we employ a quantile thresholding strategy to discard weak edges. For example, a 0.75 quantile threshold means that only the top 25% of the strongest edges are retained in the network, while the rest are set to zero. The plots are generated by varying the quantile threshold from 0.0 to 0.95 with a step size of 0.05, and computing the Global Vulnerability and Local Vulnerability at each threshold level.

In terms of biamplitude (Figure 4.11 and Figure 4.12), the following coupling types appear to have the potential to differentiate the two states at different quantile thresholds: Delta-Delta, Beta-Delta, Beta-Delta, Delta-Gamma, and Theta-Gamma. Among them, Theta-Gamma is the only one that shows higher Vulnerability during seizure periods compared to non-seizure periods, while others show the opposite trend.

Aggregated Study: To systematically evaluate the topological alterations in the brain network during ictal states, we focused on the aggregation of vulnerability metrics across the patient cohort. Specifically, we analyzed the following variables:

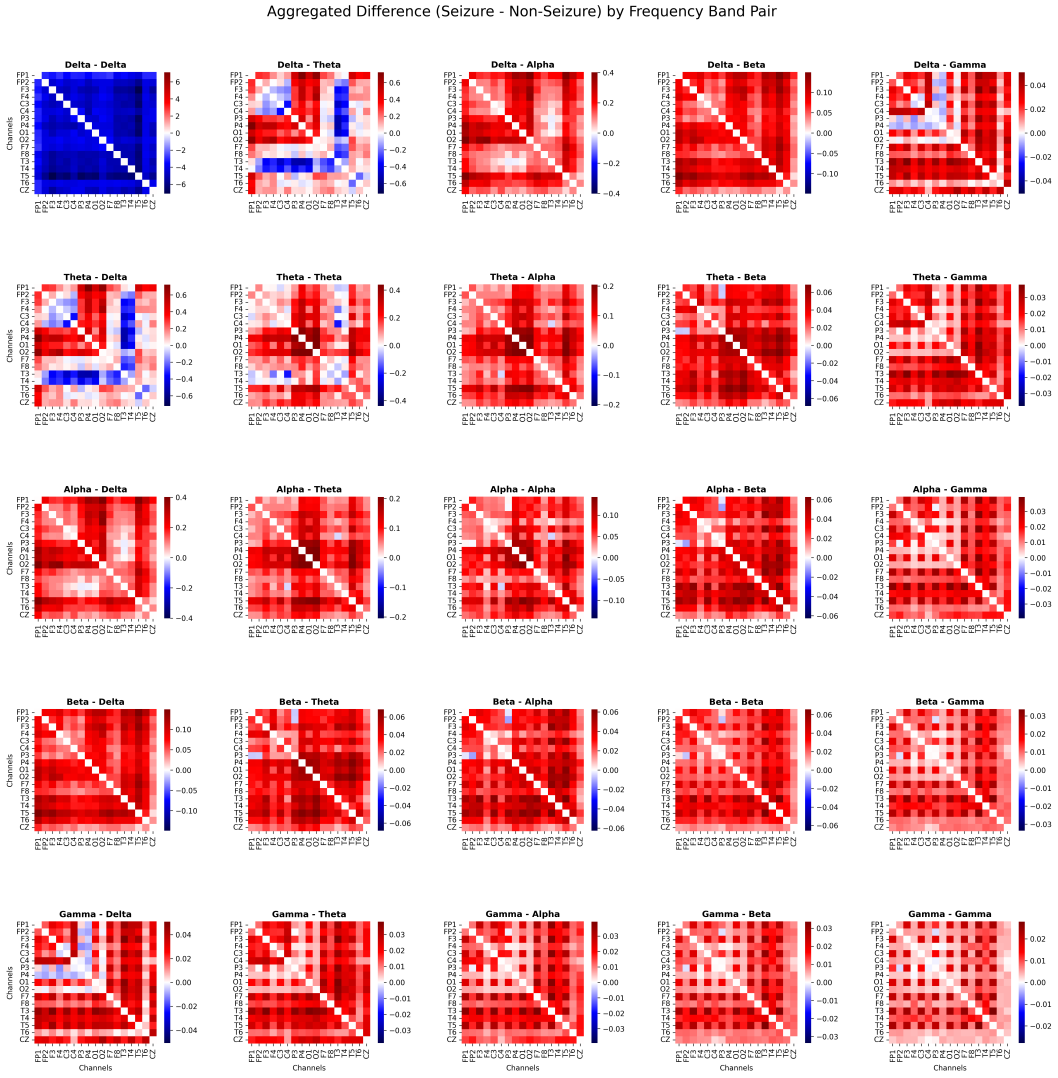

Figure 4.10: Heatmaps of Wavelet Biamplitude differences between seizure and non-seizure periods across all channel pairs and frequency band couplings.

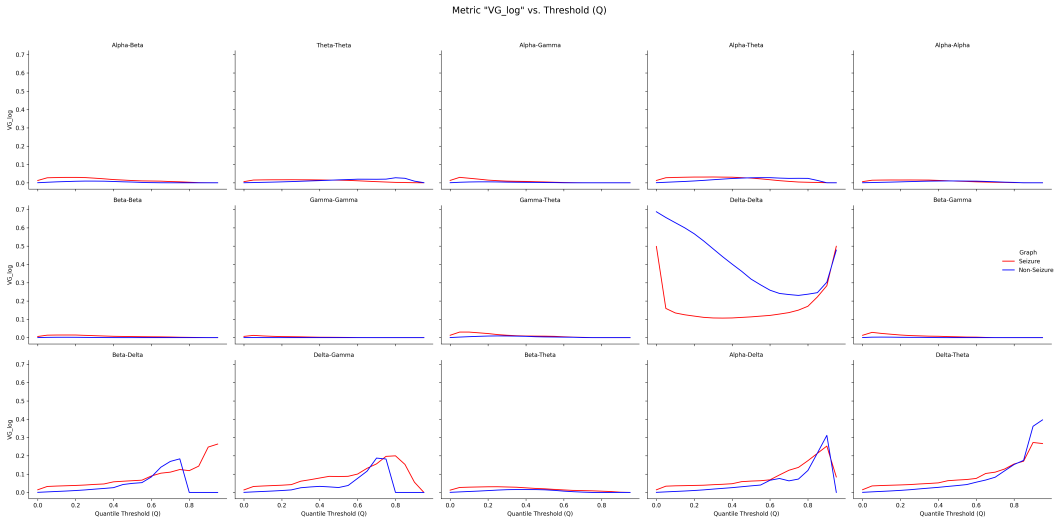

Figure 4.11: Global Vulnerability based on Wavelet Biamplitude across different frequency band couplings during seizure and non-seizure periods.

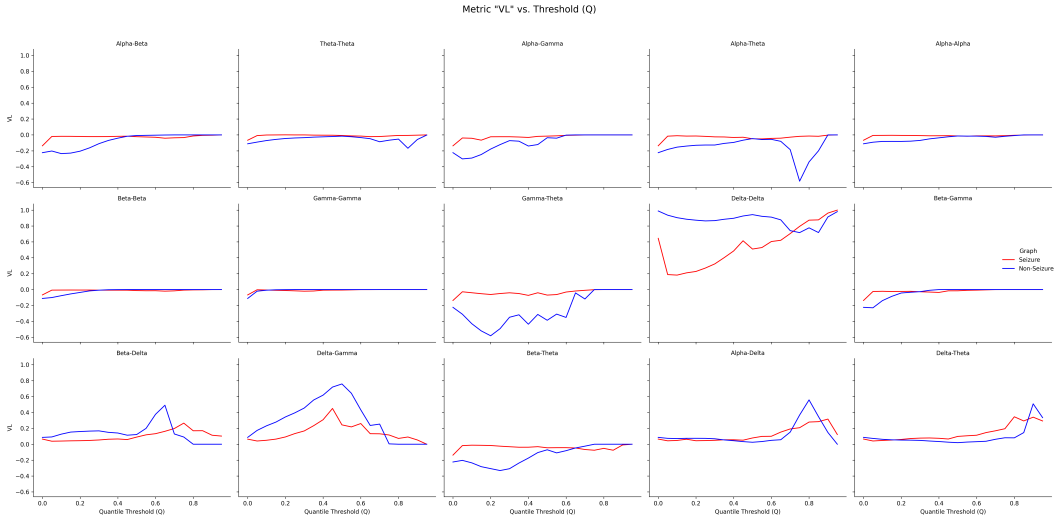

Figure 4.12: Local Vulnerability based on Wavelet Biamplitude across different frequency band couplings during seizure and non-seizure periods.

- **VG_log**: This represents the natural logarithm of the Global Vulnerability (V), i.e., VG_log = ln(V). We apply a logarithmic transformation because Global Vulnerability values typically follow a highly skewed distribution with a long tail of small values. The transformation normalizes the distribution for statistical comparison and enhances the visualization of subtle but significant changes in network efficiency.

- **VL**: This denotes the Local Vulnerability (V_{local}) as defined in Eq. (4.8). Unlike global vulnerability, local vulnerability values in our experiments exhibited a broader linear distribution, making direct visualization appropriate without transformation.

- **Cross-frequency coupling type**: This refers to the specific pairwise interaction between network layers corresponding to different frequency bands. For instance, a "Delta-Beta" coupling type implies a multilayer network constructed based on the interaction between the Delta band layer and the Beta band layer.

For each patient and each specific cross-frequency coupling type, the optimal network density threshold (Q) was identified as the value yielding the maximum relative difference between the seizure and non-seizure states. Based on these optimized parameters, we aggregated the data across the entire patient cohort to generate the statistical distributions shown in Figure 4.13. The visualizations employ box-and-whisker plots to present a comparative analysis between the two states. In these plots, the central line represents the median value of the metric across all patients, while the box edges denote the interquartile range (25th and 75th percentiles), capturing the central tendency and variability of the data. The whiskers extend to the minimum and maximum values, indicating the full range of the observed data points. The comparison is color-coded for clarity: the non-seizure (NS) periods are depicted in light blue, while the seizure (S) periods are shown in light red.

Figures 4.13a and 4.13b compare the network vulnerability between non-seizure (NS) and seizure (S) states. The boxplots illustrate the median, interquartile range, and full range (min-max) for each coupling type. We observed distinct topological shifts with significant clinical implications:

1. Robustness of the Primary Rhythm (Delta-Delta): As shown in Figure 4.13a, Delta-Delta coupling behaves differently from cross-frequency couplings. In the non-seizure state, Delta-Delta shows high vulnerability (median $\approx$ 0.30), which drops significantly during the seizure state ($\approx$ 0.14). The clinical interpretation is that a decrease in vulnerability implies an increase in robustness. This suggests that during a seizure, the pathological Delta network becomes highly redundant and hypersynchronized. From a clinical perspective, this "robustness" explains why established seizures are difficult to self-terminate or disrupt; the network

creates multiple backup pathways for signal propagation, making it resilient to focal perturbations.

2. Criticality of Cross-Frequency Bridges (Beta-Delta, Alpha-Delta): In contrast, cross-frequency couplings like Beta-Delta and Alpha-Delta show the opposite trend. Their vulnerability is low during non-seizure periods but increases sharply during seizures. The clinical interpretation is that an increase in vulnerability indicates that the network becomes heavily dependent on these specific links. This finding suggests that the interaction between low-frequency (Delta) and high-frequency (Alpha/Beta) rhythms acts as a critical "bridge" for maintaining the global seizure state. If these specific cross-frequency connections are disrupted, the efficiency of the seizure network drops dramatically. This points to a potential therapeutic target: rather than suppressing all brain activity, interventions could specifically target the decoupling of high-frequency and low-frequency interactions to destabilize the seizure network.

3. Dual Role of Delta-Gamma Coupling: The Delta-Gamma coupling shows an interesting divergence. While its *global* vulnerability is higher during seizures, its *local* vulnerability is actually higher during the *non-seizure* state. The clinical interpretation is that this suggests a state-dependent functional shift. During normal brain activity (non-seizure), Delta-Gamma coupling is crucial for maintaining local cluster integration (processing local information). However, during a seizure, these connections shift their role to support long-range, global integration. This highlights the dynamic reconfiguration of brain functional architecture, where the same frequency interactions serve different topological purposes depending on the pathological state.

In summary, the transition to a seizure state makes the main mono-frequency (Delta) network stronger and harder to break (high redundancy), but it renders the cross-frequency connections (especially between Delta and higher bands) more fragile and critical (high dependency).

4.4 Summary & Next Step

This chapter presented a dynamic functional connectivity analysis of EEG signals during seizures, moving beyond static spectral measures to capture the evolving topology of the epileptic brain using Cross-Wavelet Transform (XWT) and Wavelet Bispectrum (WB).

The XWT analysis revealed that seizure states are characterized by a generalized surge in connectivity strength and network efficiency metrics (node strength, MST weight, maximum flow) across most frequency bands. Clinically, this corresponds to a state of *pathological hyper-synchronization*, where the brain network reconfigures itself to minimize resistance, facilitating the rapid propagation of epileptic discharges across spatially distributed regions.

The WB analysis (Cross-Frequency Coupling) further uncovered the complex

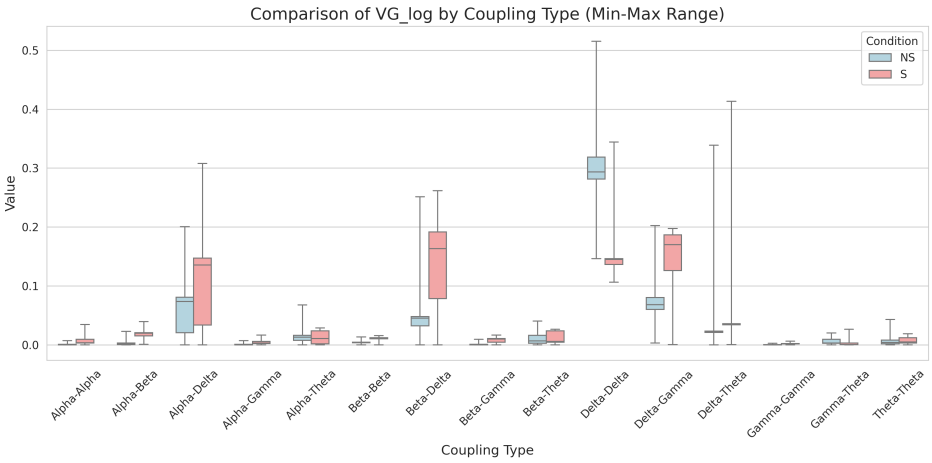

(a) Distribution of `VG_log` across different coupling types.

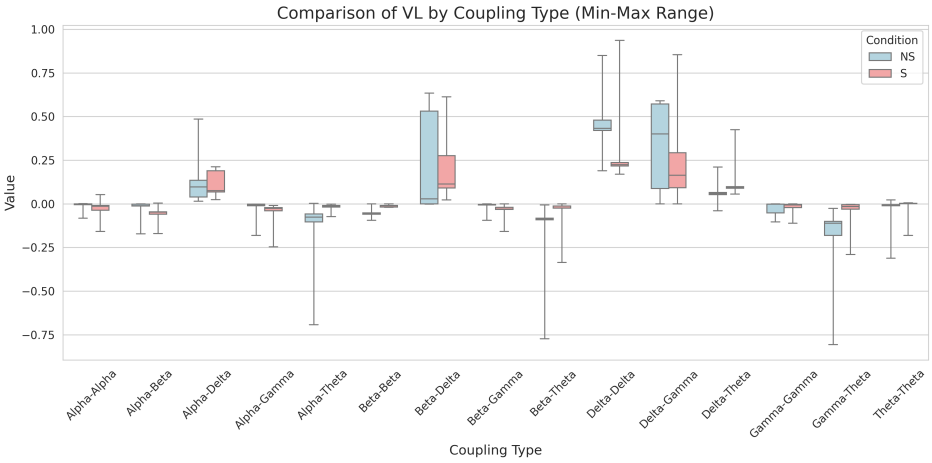

(b) Distribution of `VL` across different coupling types.

Figure 4.13: Descriptive statistics of network metrics comparing Seizure (S, light red) and Non-Seizure (NS, light blue) states.

nonlinear dynamics driving this synchronization. We observed that coupling involving high-frequency bands (Beta, Gamma) becomes significantly more prominent during seizures.

Crucially, the multilayer network vulnerability analysis provided a novel perspective on the *structural resilience* of the seizure network. We found a distinct topological shift:

- The within-frequency Delta network becomes remarkably stable (robust) during seizures due to high redundancy. Similar to a traffic grid with countless detours, the network establishes multiple backup pathways for signal propagation. This explains why established seizures are so difficult to stop naturally (self-terminate): the network is resilient to local disruptions and sustains the pathological activity through these alternative routes.

- Conversely, cross-frequency connections (e.g., between Delta and higher bands) become increasingly *fragile* (high vulnerability) and critical. This identifies these specific cross-frequency bridges as the "Achilles' heel" of the seizure network, suggesting that targeted disruption of these specific couplings could be a more effective therapeutic strategy than global suppression.

The findings in this chapter demonstrate that seizure dynamics are encoded in complex time-frequency patterns. The next logical step is to translate these analytical insights into an automated detection framework. In the following chapter, we will transition from these explicit feature extraction methods to implicit feature learning, leveraging Graph Neural Networks (GNNs) to automatically capture these spatial-temporal dependencies for robust seizure detection.

Chapter 5

Graph Wavelet Neural Networks for EEG-Based Seizure Detection

5.1 Introduction

Traditional approaches relying on feature extraction methods are often sensitive to EEG signal variability, prone to noise interference, and lack scalability due to limited dataset sizes [22]. In contrast, deep learning has demonstrated strong capabilities in addressing these challenges by automatically extracting features from raw EEG signals. CNNs and RNNs, in particular, have been widely applied for seizure detection [13, 77]. The latter capture sequential dependencies in EEG data, making them effective for time-series analysis [16]. However, these deep learning models struggle to capture spatial relationships between EEG electrodes, which are crucial for understanding brain network dynamics [17].

Graph Neural Networks (GNNs) have emerged as a powerful alternative for modeling EEG data due to their ability to represent spatial, temporal, and relational structures [10, 35, 65]. In EEG studies, GNNs have been used for applications such as emotion recognition and brain-computer interfaces, enabling a more comprehensive analysis of brain networks compared to traditional deep learning models [32]. One of the most recent models, NeuroGNN, introduced a dynamic GNN-based framework that captures multi-context correlations in EEG data, demonstrating state-of-the-art performance in seizure detection [17].

The NeuroGNN model contains several key components: graph construction, message passing and aggregation, and a final pooling step to produce the classification. It uses raw EEG signals as input and employs a default Graph Convolutional Network (GCN) layer for feature transformation. By taking raw EEG signals as input, it barely leverages frequency domain information, which is intrinsic to EEG signals. Furthermore, as it relies on a basic spectral GNN model, it fails to explore the performance benefits of message passing and aggregation mechanisms found in other spectral GNN variants for this specific application.

Building upon this foundation, this study explores the application of Graph Wavelet Neural Networks (GWNNs) in EEG-based seizure detection, marking one of the first attempts to leverage wavelet-based graph processing for EEG analysis. The key contributions of this work are as follows:

1. It demonstrates that signal preprocessing significantly improves seizure detection performance, highlighting the impact of data preparation on model effectiveness.

2. It introduces GWNNs to EEG signal analysis, utilizing their advantages in efficiency, sparsity, and localized convolution to better capture complex brain dynamics.

3. It evaluates the proposed approach on the TUSZ dataset, showing an improvement of more than 5% in recall, while maintaining AUROC performance comparable to state-of-the-art models like NeuroGNN equipped with other spectral GNN architectures.

These findings not only emphasize the importance of proper data preprocessing into the frequency domain but also illustrate the potential of GWNNs for seizure detection and wider EEG-based applications in enhancing model performance.

5.2 Proposed Method

Method Overview. Our method builds a graph-based model for EEG signals to detect seizures. It has three main steps. First, *Data Preprocessing and Representation*: We use the Fast Fourier Transform (FFT) to transform EEG signals into their frequency components. Then, we construct a graph to represent the signals. These graphs include temporal, spatial, and semantic connections. Second, *GNN Model Design*: We apply a Graph Wavelet Neural Network (GWNN) to capture important features from the graph. Third, *Prediction using the Generated Graph Representation*: We use a pooling method to combine node features. Then, we pass the final graph features into a Multi-Layer Perceptron (MLP) for classification.

The overall workflow of our method is illustrated in Fig. 5.1. The next sections explain each step in detail.

5.2.1 Data Preprocessing

EEG signals are inherently non-stationary and exhibit complex temporal dynamics. However, within a sufficiently short time window, they can be approximately regarded as stationary signals, defined as quasi-stationary [55]. McEwen and Anderson [39] found that for EEG periods of less than 32 seconds (EEG epochs), generalized stationarity is satisfied more than 50% of the time. Similarly, Isaksson

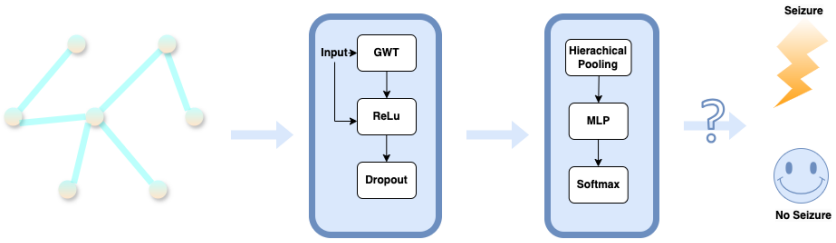

Figure 5.1: Overall workflow of our proposed method.

[24] found that in the resting state, about 90% of EEG signals maintain their characteristics within 20 seconds. Based on these empirical observations, the academic community generally accepts that for short EEG periods of about 10–20 seconds, the signal can be considered quasi-stationary when behavioral conditions remain unchanged. This "quasi-stationary" assumption is the practical basis for a large number of modern EEG analysis methods.

Based on the assumption of quasi-stationarity after dividing data into acceptable segments, the Fast Fourier Transform (FFT) efficiently converts time-domain EEG signals into their spectral components, providing both amplitude and phase information. In this research, we only utilize the amplitude spectrum, which represents signal power at different frequencies.

Rationale for Spectral Features

It is essential to clarify the methodological transition from the fine-grained time-frequency analysis in Chapter 4 to the Fourier-based preprocessing adopted in this chapter. While Chapter 4 demonstrated that Wavelet transforms offer superior resolution for characterizing the temporal evolution of seizure dynamics, using high-dimensional time-frequency maps as node features in Graph Neural Networks (GNNs) presents significant engineering challenges, including the "curse of dimensionality" and computational inefficiency.

Therefore, this chapter adopts a pragmatic approach based on the *quasi-stationary assumption* and, crucially, on the *domain knowledge* derived from our previous analysis.

- **Targeting Specific Frequency Patterns:** Our analysis in Chapter 4 revealed that seizure onsets are strongly characterized by significant energy bursts in specific high-frequency bands, particularly Beta and Gamma. FFT serves as the most direct method to extract this “energy fingerprint.”

- **Explicit Feature Extraction vs. Implicit Learning:** Asking a neural network to implicitly learn frequency decomposition and identify these spectral bursts from raw time-domain waveforms is a challenging and inefficient task. By

applying FFT, we explicitly extract these significant spectral features and feed them directly to the model.

Thus, the use of FFT is not merely a generic preprocessing step but a deliberate *feature engineering strategy*. It trades off the fine-grained temporal resolution advocated in Chapter 4 for spectral conciseness, enabling the GWNN model to focus its learning capacity on capturing the complex *spatial topologies* and connectivity patterns among electrodes.

Continuous Fourier Transform (CFT)

For a function $x(t)$ defined in the time domain t, its continuous Fourier transform $X(f)$ is defined as:

$$X(f) = \int_{-\infty}^{\infty} x(t) e^{-i2\pi f t} dt \tag{5.1}$$

where $x(t)$ is the signal in the time domain, and $X(f)$ is its representation in the frequency domain. This integral correlates the time-domain signal $x(t)$ at every point with a specific complex exponential function of frequency f (which can be seen as a combination of sine and cosine waves), and then integrates over the entire time axis to calculate the "weight" of that frequency component in the original signal.

Discrete Fourier Transform (DFT) and Fast Fourier Transform (FFT)

For a finite-length discrete sequence $x[n]$ composed of N samples (where $n = 0, 1, \ldots, N-1$), its Discrete Fourier Transform (DFT) $X[k]$ (where $k = 0, 1, \ldots, N-1$) is defined as:

$$X[k] = \sum_{n=0}^{N-1} x[n] \cdot e^{-i2\pi kn/N} \tag{5.2}$$

To compute the entire DFT for a sequence of length N, a total of $N \times N = N^2$ complex multiplications and $N \times (N-1)$ complex additions are needed. This gives the DFT a computational complexity of $O(N^2)$.

To reduce the computational burden, a series of Fast Fourier Transform (FFT) algorithms were developed, among which the Cooley–Tukey algorithm is the most common. By taking advantage of a "divide and conquer" strategy, it achieves a computational complexity of $O(N \log N)$.

5.2.2 Data Representation

Following [17], EEG signals are represented as a graph by encoding temporal, spatial, and semantic correlations. We explicitly define the input EEG data as a matrix $\mathbf{X} \in \mathbb{R}^{N \times T}$, where N denotes the number of EEG electrodes (channels) and T denotes the number of time points (sequence length).

Node Features Construction

By averaging the signals according to the brain regions in which their electrodes reside, 6 meta-nodes are generated, representing the aggregational activities in a certain brain region. Combining these with the signals of the original electrodes provides a multi-resolution representation of brain activities. The shape of the augmented data is $\mathbf{X}' \in \mathbb{R}^{N' \times T}$ where $N' = N + 6$.

Temporal embeddings are extracted via a Bidirectional Gated Recurrent Unit (BiGRU) [21]. Two hidden states are generated for each node, $\mathbf{h}_{f,i} \in \mathbb{R}^M$ and $\mathbf{h}_{b,i} \in \mathbb{R}^M$, containing forward temporal dynamics and backward temporal dynamics respectively, where M is the hidden dimension. Concatenating them generates the temporal embedding matrix $\mathbf{C} \in \mathbb{R}^{N' \times 2M}$.

Semantic embeddings are derived from a pre-trained language model based on Brodmann area mappings [80] corresponding to the electrode locations. The semantic embedding matrix has a shape of $\mathbf{U} \in \mathbb{R}^{N' \times K}$, where K is the semantic dimensionality.

Concatenating the above embeddings produces the final node embedding matrix with a shape of $\mathbf{V} \in \mathbb{R}^{N' \times (2M+K)}$.

Edge Construction

To comprehensively model the dependencies between EEG channels, we construct the graph adjacency matrix by integrating correlations from three distinct contexts: semantic, spatial, and temporal. This part inherited from NeuroGNN [17]. The construction of the specific similarity matrices is defined as follows:

1. Semantic Similarity Matrix ($\mathcal{S}_E$) This matrix captures the functional relationships between brain regions based on domain knowledge. Let $\mathbf{u}_i$ and $\mathbf{u}_j$ denote the semantic embedding vectors for nodes i and j, which are derived from the pre-trained language model processing the functional descriptions of the corresponding brain areas. The entries of $\mathcal{S}_E$ are computed using the cosine similarity:

$$\mathcal{S}_E(i,j) = \frac{\mathbf{u}_i \cdot \mathbf{u}_j}{\|\mathbf{u}_i\| \|\mathbf{u}_j\|} \tag{5.3}$$

Values close to 1 indicate high semantic relevance between the regions.

2. Spatial Similarity Matrix ($\mathcal{S}_S$) This matrix encodes the physical proximity of the electrodes on the scalp. Let $\mathbf{p}_i$ and $\mathbf{p}_j$ represent the 3D spatial coordinates of electrodes i and j. The spatial similarity is derived from the Euclidean distance $d_{ij} = \|\mathbf{p}_i - \mathbf{p}_j\|_2$, transformed by a Gaussian kernel to map distances to similarity weights:

$$\mathcal{S}_S(i,j) = \exp\left(-\frac{d_{ij}^2}{2\sigma^2}\right) \tag{5.4}$$

where σ is a scaling parameter controlling the sparsity of the spatial connections.

3. Temporal Similarity Matrix ($\mathcal{S}_T$) Unlike the static spatial and semantic matrices, $\mathcal{S}_T$ captures the dynamic temporal dependencies between signals. It is generated via a Multi-Head Attention mechanism [71]. Given the temporal node embeddings $\mathbf{C}$ (output from the BiGRU), we compute Queries ($\mathbf{Q}$) and Keys ($\mathbf{K}$) through linear transformations. The temporal similarity matrix is obtained via the self-attention mechanism:

$$\mathcal{S}_T = \text{Softmax}\left(\frac{\mathbf{Q}\mathbf{K}^\top}{\sqrt{d_k}}\right) \tag{5.5}$$

where d_k is the dimension of the key vectors. This matrix dynamically adjusts edge weights based on the instantaneous temporal correlation between channels.

Fusion Mechanism The final adjacency matrix is synthesized by fusing these three components. First, the static similarities (Semantic and Spatial) are combined using a gate mechanism with a learnable parameter $\alpha \in [0, 1]$:

$$\mathcal{S}_{\text{Gate}} = (1 - \alpha)\mathcal{S}_E + \alpha\mathcal{S}_S \tag{5.6}$$

This allows the model to adaptively balance the importance of physical distance versus functional semantic relationships. Finally, this static structural prior is modulated by the dynamic temporal correlations via an element-wise product to produce the final adjacency matrix $\mathcal{S}'$:

$$\mathcal{S}' = \mathcal{S}_{\text{Gate}} \odot \mathcal{S}_T, \tag{5.7}$$

5.2.3 GNN Model Design

Graph Wavelet Transform

The graph wavelet basis is defined as:

$$\psi_s = UG_sU^\top, \tag{5.8}$$

where U is the Laplacian eigenvector matrix and $G_s = \text{diag}(g(s\lambda_1), \ldots, g(s\lambda_n))$ is a scaling matrix with $g(s\lambda_i) = e^{s\lambda_i}$ as a common heat kernel.

The wavelet transform of a signal x is given by:

$$\hat{x} = \psi_s^{-1}x, \tag{5.9}$$

where ψ_s^{-1} is the inverse wavelet transform.

The wavelet-based convolution is defined as:

$$x *_g y = \psi_s\left((\psi_s^{-1}y) \circ (\psi_s^{-1}x)\right), \tag{5.10}$$

where $\circ$ denotes the Hadamard product. This approach retains spatial and spectral efficiency, making it particularly advantageous for EEG-based seizure detection [74].

Graph Wavelet Neural Network in Seizure Detection

We employ a single-layer Graph Wavelet Neural Network (GWNN) [74] as the initial feature transformation stage before hierarchical pooling. The transformation scale s is treated as a hyperparameter to control the diffusion of signals across the graph.

The GWNN layer is formulated as:

$$X^{\text{out}}_{[:,j]} = \text{Dropout}\Big(\text{ReLU}\big(\text{LayerNorm}(\psi_s \sum_{i=1}^{p} F_{i,j}\psi_s^{-1} X^{\text{in}}_{[:,i]} + X^{\text{in}})\big), p\Big). \tag{5.11}$$

where X^{in} is the input feature matrix, ψ_s represents the graph wavelet bases at scale s, and ψ_s^{-1} is the inverse wavelet transform matrix. The learnable diagonal filter matrix $F_{i,j}$ is optimized during training.

In this formulation, a residual connection is incorporated by adding X^{in} to the transformed feature matrix before applying layer normalization, which ensures stable feature distributions. The output is then passed through a ReLU activation function to introduce non-linearity, followed by dropout with probability p to mitigate overfitting.

Alternative Spectral GNN Models for Comparison

We now briefly introduce two other spectral GNN models used as baselines for comparison in this study.

Graph Convolutional Network (GCN): As one of the most famous and influential models in the field of graph neural networks, the success of the Graph Convolutional Network (GCN) lies in simplifying complex spectral graph convolution theory into an efficient, scalable, and easy-to-implement framework. This section provides an in-depth deconstruction of the GCN model proposed by Kipf and Welling [29] and establishes it as a baseline for subsequent discussions.

The core computation of each layer in a GCN can be expressed by the following formula:

$$\mathbf{H}^{(l+1)} = \sigma\left(\tilde{\mathbf{D}}^{-\frac{1}{2}}\tilde{\mathbf{A}}\tilde{\mathbf{D}}^{-\frac{1}{2}}\mathbf{H}^{(l)}\mathbf{W}^{(l)}\right) \tag{5.12}$$

where $\mathbf{H}^{(l)}$ is the node representation matrix of the l-th layer, with $\mathbf{H}^{(0)} = \mathbf{X}$. $\tilde{\mathbf{A}} = \mathbf{A}+\mathbf{I}$ is the adjacency matrix with self-loops added, where $\mathbf{I}$ is the identity matrix. Adding self-loops ensures that a node's own features are considered during information aggregation. $\tilde{\mathbf{D}}$ is the diagonal degree matrix of $\tilde{\mathbf{A}}$, where $\tilde{\mathbf{D}}_{ii} = \sum_j \tilde{\mathbf{A}}_{ij}$. $\mathbf{W}^{(l)}$ is the trainable weight matrix of the l-th layer. $\sigma(\cdot)$ is a non-linear activation function, such as ReLU [29].

This operation can be intuitively understood as a two-step process: First, a linear transformation is performed on the features of each node via $\mathbf{H}^{(l)}\mathbf{W}^{(l)}$; then,

the transformed features are aggregated onto their neighboring nodes by left-multiplying with the symmetrically normalized adjacency matrix $\tilde{\mathbf{D}}^{-\frac{1}{2}}\tilde{\mathbf{A}}\tilde{\mathbf{D}}^{-\frac{1}{2}}$. This normalization step is crucial for stabilizing the training process [29].

Spectral Graph Temporal Network (StemGNN): Unlike GCN, which pursues universality and simplicity, the Spectral Graph Temporal Network (StemGNN) is a highly specialized architecture designed to solve complex multi-variable time-series prediction problems. It demonstrates how GNNs can address unique challenges posed by specific domains, such as dynamic systems, through sophisticated architectural design [6].

The core operation within the StemGNN module can be summarized by the following formula:

$$\mathbf{Z}_j = GF^{-1}\left(\sum_i g_{\theta_{ij}}(\Lambda_i)\mathcal{S}(GF(\mathbf{X}_i))\right) \tag{5.13}$$

where $\mathbf{X}_i$ is the input channel, $\mathbf{Z}_j$ is the output channel, GF and GF^{-1} are the Graph Fourier Transform (GFT) and its inverse, respectively, $\mathcal{S}$ represents a latent spectral sequence unit that includes the DFT, a 1D convolution, and the inverse DFT, and $g_{\theta_{ij}}$ is a graph convolution kernel learned in the graph spectral domain. This formula clearly shows how the model first enters the graph spectral domain via the GFT, then processes the data in the temporal spectral domain via $\mathcal{S}$, and finally returns to the original data space through the inverse transform [6].

5.2.4 Prediction using the Generated Graph Representation

After the GWNN layer, the node features are updated to $\mathbf{V}' \in \mathbb{R}^{N' \times Z}$, where Z is the embedding dimension. Next, a hierarchical pooling mechanism aggregates the refined node representations into a single graph embedding vector [17]. First, within each brain region, the embeddings of EEG nodes are aggregated through a max-pooling operation. Likewise, max-pooling is performed on all meta-nodes to build a single embedding vector for the meta-nodes. These pooled embeddings are concatenated together to form a collective representation of region-level and meta-node-level node information. A mean-pooling operation is performed on the concatenated representation to obtain a graph embedding vector that encapsulates key graph information, denoted as $\mathbf{g} \in \mathbb{R}^Z$ [17].

Finally, $\mathbf{g}$ is passed through an MLP with Softmax activation for classification, using cross-entropy loss for training [17].

5.3 Experiments and Results

5.3.1 Dataset Used

Our experiments use the Temple University Hospital Seizure Detection Corpus (TUH-SD) Version 2.0.3, released on February 7, 2024. Since this study focuses solely on seizure detection rather than seizure type classification, we utilize only the `.csv_bi` files, which provide binary annotations: *bckg* (background) and *seiz* (seizure).

5.3.2 Evaluation Metrics

We evaluate model performance using AUCROC and recall. AUCROC reflects overall discrimination ability. Recall is crucial for seizure detection, ensuring minimal missed events, which is vital for clinical applications.

AUCROC

AUCROC is an important metric for evaluating the performance of binary classification models. It comprehensively measures the trade-off between "correctly identifying positive examples" and "erroneously identifying negative examples as positive examples" under all possible classification thresholds.

ROC Curve: The ROC curve, short for "Receiver Operating Characteristic curve," is a tool that graphically displays the performance of a classification model. Its x-axis and y-axis are:

X-axis: False Positive Rate (FPR)

$$\text{FPR} = \frac{\text{FP}}{\text{FP} + \text{TN}} \quad \text{(FP: False Positive, TN: True Negative)} \tag{5.14}$$

The proportion of all actual negative samples that are incorrectly predicted as positive by the model. A lower FPR indicates a more accurate judgment of negative samples by the model.

Y-axis: True Positive Rate (TPR)

$$\text{TPR} = \frac{\text{TP}}{\text{TP} + \text{FN}} \quad \text{(TP: True Positive, FN: False Negative)} \tag{5.15}$$

The proportion of all actual positive samples that are correctly predicted as positive by the model. This metric is also called *Recall* or *Sensitivity*. A higher TPR indicates a stronger ability of the model to identify positive samples.

AUC: AUC refers to the Area Under the ROC Curve. It is a numerical value between 0 and 1 that provides a single scalar evaluation of a model's performance.

$AUC = 1$: Perfect classifier. At some threshold, it can perfectly distinguish between all positive and negative samples.

$AUC = 0.5$: Random classifier. The model's predictive performance is equivalent to random guessing.

$AUC < 0.5$: The classifier's performance is worse than random guessing.

AUC has a very important probabilistic interpretation: it is equal to the probability that a randomly chosen positive sample will have a higher predicted probability than a randomly chosen negative sample. It is independent of a specific classification threshold, which is very important in practical applications, especially when the proportions of positive and negative samples are imbalanced.

5.3.3 Baseline Comparison

We evaluate our model against two baselines: GCN and StemGNN [6], within the NeuroGNN framework. GCN is a widely used graph-based model for learning spatial dependencies in EEG signals. The original NeuroGNN study already benchmarked against LSTM, Dense-CNN, CNN-LSTM, Corr-DCRNN, and Dist-DCRNN, demonstrating its superior performance. Therefore, we do not include these baselines in this study.

5.3.4 Performance Evaluation on Full TUSZ Imbalanced Datasets

While the previous experiments on balanced datasets verified the fundamental capability of our model, clinical scenarios have another challenge. In real-world clinical triage, the number of negative samples (normal or non-seizure segments) is enormously larger than positive samples (seizure segments). To evaluate the robustness of the proposed GWNN model in clinical settings, we extended our evaluation to the full TUSZ dataset.

In this setting, the ratio of positive to negative samples reaches beyond 1:11 in training set (train), 1:12 in validation set (dev) and 1:8 in test set (eval), as concluded in Table 5.1, exhibiting a significant class imbalance. We compared GWNN against the baseline model (GCN, employed in NeuroGNN) using AUROC, Max F1 score, and the sensitivity derived at the threshold of Max F1.

5.3.5 Results

We evaluate seizure detection performance under a balanced dataset setting (50% seizure and 50% non-seizure samples in both training and testing). The results are presented separately for models with and without FFT preprocessing.

Dataset Split	Non-Seizure	Seizure	Total Samples	Ratio (Pos : Neg)
Training Set	49,236	4,306	53,542	1 : 11.43
Validation Set	23,853	1,953	25,806	1 : 12.21
Test Set	6,734	805	7,539	1 : 8.37
Total	**79,823**	**7,064**	**86,887**	**1 : 11.30**

Table 5.1: Statistics of the dataset splits and class distribution. The dataset exhibits a significant class imbalance across all subsets.

GCN	Rec.	AUC
With FFT	0.898	0.758
Without FFT	1.000	0.612

(a) GCN performance comparison.

StemGNN	Rec.	AUC
With FFT	0.887	0.757
Without FFT	0.961	0.613

(b) StemGNN performance comparison.

GWNN	Rec.	AUC
With FFT	0.942	0.757
Without FFT	0.955	0.612

(c) GWNN performance comparison.

Table 5.2: Performance comparison of GCN, StemGNN, and GWNN with and without FFT preprocessing.

Comparison of Performance with and without FFT Preprocessing

Table 5.2 compares the performance of GCN, StemGNN, and GWNN with and without FFT preprocessing. The results show that FFT preprocessing significantly improves model performance, with all models achieving higher AUCROC scores when FFT is applied. Conversely, recall rates are slightly lower with FFT preprocessing.

Comparison of Model Performance

Table 5.3 presents the performance of different models. Among them, GWNN achieves the highest recall without affecting AUCROC, demonstrating its superior ability to balance seizure detection sensitivity and overall discrimination capability.

To quantify the improvement of GWNN over other models in recall, we introduce a relative improvement column.

Influence of GWNN's Scale Parameter

Under the default dropout rate of 0, we investigate the impact of the GWNN scale parameter s on model performance. In our implementation, s is treated as a hyperparameter, generating a graph wavelet basis pair ψ_s and ψ_{-s} at scale s and $-s$, respectively.

Model	Recall	AUCROC	GWNN Improvement in Recall (%)
GCN	0.898	0.758	+4.9
StemGNN	0.887	0.757	+6.2
GWNN	**0.942**	0.757	-

Table 5.3: Performance comparison of models with FFT preprocessing, including relative improvement of GWNN.

Scale	Recall	AUROC
1	0.905	0.752
2	0.913	0.751
4	0.874	0.750
6	0.906	0.752
8	0.887	0.757
10	0.838	0.752
20	0.875	0.755

Table 5.4: Recall and AUROC under different GWNN scale parameters.

In Table 5.4, we present the recall and AUCROC for various scale values. The results indicate that the model's performance is relatively stable across different scales, with minor fluctuations in recall and AUCROC. The best recall of 0.913 is achieved at scale 2, while the highest AUCROC of 0.757 occurs at scale 8.

In order to visualize the effect of scale on the graph wavelet basis, we plot the line graphs of recall and AUROC values for different scales in Fig. 5.2. The x-axis represents the chosen s value for the scale parameter to generate a scale pair of $-s$ and s, while the y-axis represents the corresponding recall and AUROC values. The blue line represents recall, while the orange line represents AUROC. The graph shows that both metrics exhibit fluctuations across different scales, with no clear linear trend. This suggests that the choice of scale parameter has a nuanced impact on model performance, and optimal values may depend on specific data characteristics. In addition, compared to AUROC, recall values exhibit more fluctuations and less stability.

Influence of GWNN's Dropout Rate

We explore the effect of different dropout rates on GWNN performance. Dropout is a regularization technique that randomly sets a fraction of input units to zero during training, preventing overfitting and improving generalization. In Table 5.5, we present the recall and AUCROC for various dropout rates. The results

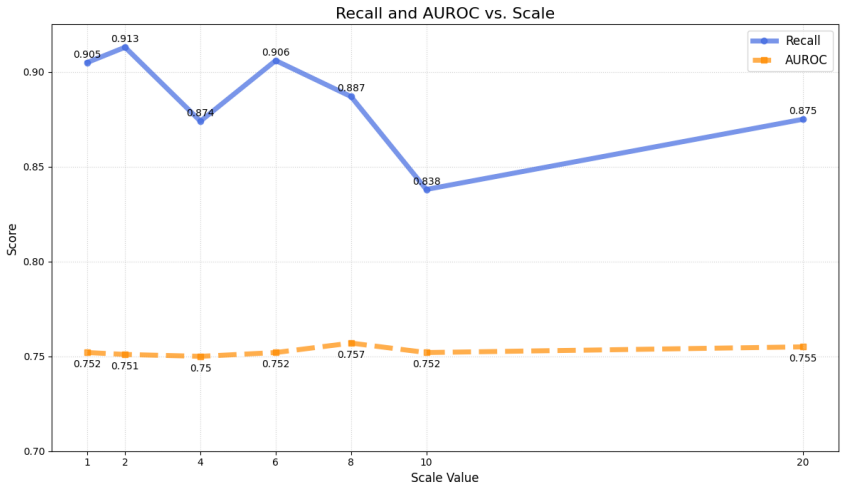

Figure 5.2: Effect of GWNN scale parameter on recall and AUROC.

Dropout Rate	Recall	AUROC
0	0.905	0.752
0.3	0.942	0.754

Table 5.5: Recall and AUROC under different GWNN dropout rates.

indicate that a dropout rate of 0.3 yields the best recall of 0.942, while maintaining a comparable AUCROC of 0.754. This suggests that moderate dropout effectively balances model complexity and generalization.

Combining the optimal scale of 8 and dropout rate of 0.3, we achieve the best overall performance with a recall of 0.942 and AUCROC of 0.757.

Full TUSZ Imbalanced Dataset

The comparative results on the imbalanced dataset are summarized in Table 5.6. Despite the challenging distribution shift of the positive-negtive sample ratios, GWNN consistently outperformed the baseline model.

Specifically, GWNN achieved an AUROC of 0.837, which is 0.722% higher than GCN. Most importantly, at the optimal decision threshold (determined by the maximum F1 score), GWNN had a recall of 0.574. This indicates that even when optimizing for the overall trade-off between precision and recall, our model retains a superior ability to capture true positive cases compared to the baseline, remaining consistent with the results observed in the balanced dataset experiments.

Model	Recall (at Max F1)	AUROC	GWNN Improvement in Recall(%)
GCN (Baseline)	0.504	0.831	+13.9
GWNN (Ours)	**0.574**	**0.837**	

Table 5.6: Performance comparison on the full TUSZ imbalanced dataset.

5.4 Discussion

5.4.1 Interpretation of Results

Data Preprocessing Impact

The results indicate that incorporating FFT preprocessing improves the model's ability to distinguish between seizure and non-seizure events, as reflected in the AUCROC scores. While models without FFT achieved higher recall, their lower AUCROC suggests an increased rate of false positives. This trade-off highlights the importance of frequency-domain features in enhancing overall model robustness and reliability.

GNN Architecture Comparison

Among the tested architectures, GWNN demonstrated the best balance between recall and AUCROC, highlighting the advantages of graph wavelet-based feature extraction for seizure detection. Compared to AUROC, which demonstrates a certain extent of stability among models, recall shows more significant variations, indicating that GWNN is particularly effective in capturing seizure-related patterns while minimizing missed detections.

GCN simplifies the calculation by approximating complex spectral graph theory into a simple, efficient aggregation operation that resembles methods in the spatial domain [29]. This extreme simplification makes it an available, usable, and even powerful tool, which turns out to be a key factor in the popularization of GNNs. It operates in a Fourier domain simplified by polynomial approximation, and its filters are strictly limited to a first-order polynomial of the Laplacian operator [29]. While this approach is computationally inexpensive, it sometimes has the tendency to sacrifice the expressive power of the filters, enabling it to capture only very local neighborhood information.

The philosophy of StemGNN, conversely, is to customize a highly complex solution for a specific problem. It focuses on the spatio-temporal properties of multivariate time-series forecasting [6]. By fusing GFT and DFT, it constructs a powerful, specialized architecture and is designed to sacrifice higher computational costs to achieve state-of-the-art performance in its very specific applications [6].

Additionally, based on the results, using it on the dataset used in this study for a classification task may lead to issues with overfitting.

GWNN, in contrast, achieves a balance between simplicity and specialization, as well as efficiency and performance. It returns to the spectral domain empowered by wavelets, a powerful multi-resolution mathematical tool [74]. Its objective is to maintain the theoretical interpretability of spectral methods while effectively reducing computational complexity by leveraging excellent characteristics such as sparsity and localization. This allows the model to learn more expressive and interpretable filters capable of capturing graph structural information at different scales [74].

5.4.2 Strengths and Weaknesses of the Approach

Our approach uses Graph Wavelet Neural Networks (GWNNs) to model EEG data for seizure detection. This method benefits from multi-scale feature extraction abilities and the localized spectral properties of wavelets, which traditional GCNs lack due to their fixed receptive fields. Additionally, our model effectively integrates multi-context information, enhancing seizure detection accuracy.

However, some limitations remain. First, the reliance on FFT preprocessing may introduce additional computational overhead, which could be a concern for real-time applications. Second, while our method outperforms conventional graph models, its effectiveness may depend on the dataset's electrode configuration and noise levels.

Finally, in this study, we treat the GWNN scale parameter as a hyperparameter, which requires manual tuning. In addition, the number of wavelets is fixed at $-s$ and s, which largely limits the expressive power and the capacity to capture multi-scale features of the EEG signal networks. Future work could explore adaptive mechanisms to optimize this parameter during training by leveraging attention mechanisms or learnable parameters. Furthermore, incorporating multiple scales simultaneously could enhance the model's ability to capture complex brain dynamics.

5.4.3 Clinical Applicability

The proposed approach is promising for real-world clinical applications, particularly in automated seizure monitoring systems.

Seizures can often be easily missed. For example, nonconvulsive and subclinical seizure detection requires high sensitivity, especially in critically ill patients in the intensive care unit (ICU) because they have few or no external clinical symptoms (such as convulsions) [55]. In the ICU, the vast majority (approximately 75%) of seizures are "subclinical" and are often unrecognized by bedside caregivers, usually discovered only by reviewing time-synchronized EEG videos [55]. If the patient fails to regain consciousness after the convulsive seizure has stopped, it is clinically

difficult to distinguish whether they are in a benign late stage of the seizure or are experiencing dangerous non-convulsive status epilepticus (NCSE). At this time, EEG is the only diagnostic tool [55]. Additionally, the symptoms of neonatal seizures are very subtle and atypical, and can easily be confused with normal physiological events such as shaking and startling in newborns. It is very easy to miss a diagnosis if EEG monitoring is not used [41, 45]. Furthermore, patients themselves often seriously underreport their attacks due to amnesia, which prevents doctors from accurately assessing their condition [55].

From a practical perspective, the conclusion is that high recall ensures that seizure events are rarely missed, which is crucial for timely medical intervention. By using GWNNs, our model offers an effective solution that could be integrated into wearable EEG devices or hospital monitoring systems.

5.4.4 Robustness Against Class Imbalance

The transition from the balanced dataset to the full, highly imbalanced TUSZ dataset provides a rigorous stress test for model robustness. It is important to note that *StemGNN was excluded* from this full-scale evaluation. StemGNN possesses over 100 million parameters, three orders of magnitude larger than the lightweight GCN and GWNN (approximately 100k parameters). Given that StemGNN had the lowest performance even on the smaller balanced dataset (Table 5.3), its deployment on the full dataset proved computationally prohibitive in terms of training time and hardware requirements without offering significant performance gains.

Comparing the performance between the balanced (Table 5.3) and imbalanced (Table 5.6) settings reveals the following trends:

1. **Ranking Quality and Easy Negatives (AUROC Increase):** Counter-intuitively, the AUROC scores for both models increased significantly in the imbalanced setting (rising from ~0.75 to ~0.83). This phenomenon can be attributed to the nature of the added negative samples. The down-sampling process in the balanced dataset likely retained "hard" negatives that spectrally resembled seizures. Conversely, the full dataset introduces a vast volume of "easy" negatives (clear background activity). Both models successfully ranked these distinct background signals with low seizure probabilities, thereby boosting the overall area under the curve.

2. **Recall Collapse (Recall Analysis):** While ranking quality improved, the absolute Recall (at Max F1 threshold) dropped largely for both models. This is a mathematically expected consequence of optimizing for F1 in an imbalanced scenario: to prevent precision from collapsing due to the overwhelming number of negative samples, the decision threshold must be raised, inevitably sacrificing recall.

3. **Horizontal Comparison:** Under these harsh conditions, the baseline GCN struggled significantly, with its recall dropping to 0.504. This indicates that standard graph convolutions failed to effectively separate seizure features from the high-density noise, resulting in a detection rate barely above random chance for the identified threshold. In contrast, GWNN demonstrated superior resilience, maintaining a recall of 0.574. While the absolute value is lower than in the balanced setting, GWNN achieved a relative improvement of 13.9% over the GCN baseline. This suggests that the graph wavelet mechanism acts as a robust band-pass filter, preserving critical seizure information that gets washed out by the over-smoothing effect of standard GCNs in high-noise environments.

Clinical Implications. From a patient safety perspective, the relative superiority of GWNN is clinically vital. In a triage system, a recall of 0.504 (GCN) implies missing nearly half of the seizure events, which is unacceptable. GWNN's ability to recover significantly more true positives (+13.9%) highlights its potential as a safer backbone for automated epilepsy monitoring. However, it must be acknowledged that an absolute recall of 0.574 is still below the stringent standards required for standalone clinical diagnosis, where missed detections can have severe consequences. This performance gap indicates that architectural improvements alone—while effective—are insufficient to fully neutralize the bias introduced by extreme class imbalance. Consequently, addressing this data disparity remains the primary objective for our future research to achieve a clinically deployable solution.

Chapter 6

Conclusions and Future Work

6.1 Summary of Research

This thesis aimed to enhance automated seizure detection from complex, non-stationary EEG signals by integrating advanced time-frequency analysis with graph-based deep learning models. Traditional methods, ranging from manual feature engineering to standard deep learning architectures like CNNs and RNNs, often struggle to capture the intricate spatio-temporal and relational dynamics inherent in brain networks during epileptic events. This research successfully demonstrated that a hybrid approach, leveraging both principled signal processing techniques and specialized Graph Neural Network (GNN) architectures, can yield significant improvements in detection performance.

6.2 Key Contributions

The primary contributions of this work are twofold, addressing both analytical and methodological aspects of seizure detection.

6.2.1 Analytical Contributions: Dynamic Connectivity

First, we conducted a comprehensive brain network analysis in the time-frequency domain using Cross-Wavelet Transform (XWT) and Wavelet Bispectrum (WB) to model both linear and nonlinear effective connectivity. Our findings revealed statistically significant changes in network synchronization during seizures, particularly highlighting the critical role of higher frequency bands (beta and gamma) in seizure dynamics. Notably, this study is among the first to successfully apply these dynamic connectivity analyses to non-invasive scalp EEG data, demonstrating their feasibility for investigating seizure mechanisms beyond the confines of intracranial recordings.

6.2.2 Methodological Contributions: GWNN Framework

Second, this research systematically evaluated and compared several spectral GNN architectures within the NeuroGNN framework, leading to two key insights. We established that data preprocessing using the Fast Fourier Transform (FFT) is crucial, as it significantly boosts the discriminative power (AUROC) across all tested models, resulting in more robust classification. Most importantly, we demonstrated that the Graph Wavelet Neural Network (GWNN) achieves a superior balance between sensitivity and overall performance. Compared to baseline models such as GCN and StemGNN, GWNN improved recall by over 5% while maintaining a highly competitive AUROC. This enhancement in recall is clinically vital, as it directly translates to minimizing missed seizure events. The success of GWNN suggests that its ability to perform multi-scale, localized analysis via its wavelet basis provides a more expressive and effective framework than the simplified approximations of GCN or the highly specialized design of StemGNN for this specific task.

6.3 Limitations

Despite these promising results, this study acknowledges several limitations. The reliance on FFT preprocessing in the classification framework, while effective for extracting energy features, introduces additional computational overhead compared to raw signal processing and relies on a quasi-stationary assumption that may simplify transient dynamics. Furthermore, the scale parameter in the GWNN architecture was treated as a fixed hyperparameter, limiting the model's capacity to adaptively capture the multi-scale features inherent in diverse EEG signals. Additionally, the findings are based on a single, albeit extensive, dataset (TUSZ); thus, further validation on more heterogeneous datasets is required to ensure generalizability.

6.4 Future Directions

Building upon the insights and limitations of this work, future research should proceed in several promising directions.

6.4.1 Optimization of GWNN Architecture

A key priority is the optimization of the GWNN architecture by incorporating multiple, learnable scales—potentially guided by an attention mechanism—to create a more dynamic and powerful feature extraction process. This would allow the model to automatically adapt to the varying frequency characteristics of different seizure types.

6.4.2 Integration of Time-Frequency Features into GNNs

While the FFT-based approach in Chapter 5 demonstrated success under the quasi-stationary assumption, it inevitably simplifies the complex non-stationary dynamics of seizures. A promising direction is to bridge the gap between the findings in Chapter 4 and Chapter 5. Future work should explore using the advanced time-frequency features extracted in Chapter 4—specifically the *Wavelet Bispectrum* and *Cross-Frequency Coupling (CFC) metrics*—as input node features for the Graph Neural Network. By replacing the static FFT spectrum with these dynamic connectivity features, the model could leverage the GNN's spatial aggregation capabilities without sacrificing the temporal resolution required to capture non-stationary events. This hybrid approach aims to combine the "best of both worlds": the dynamic sensitivity of wavelets and the topological learning power of graph neural networks.

6.4.3 Validation on Heterogeneous and Imbalanced Datasets

Finally, expanding the evaluation to include a wider range of EEG datasets will be essential for developing a truly robust and clinically applicable model. Specifically, future work aims to improve recall at the maximal F1 score on the full TUH dataset (100%) to enhance model robustness on imbalanced dataset. Furthermore, incorporating external datasets with different recording conditions will be critical to verify the model's generalization capabilities across different patient demographics and hardware configurations. By addressing these aspects, we can advance closer to creating automated systems that are not only accurate and efficient but also trusted tools in clinical practice.

Bibliography

[1] T. N. Alotaiby, S. A. Alshebeili, T. Alshawi, G. Muhammad, and M. Alshenaifi, *EEG seizure detection and prediction algorithms: a survey*, EURASIP Journal on Advances in Signal Processing, 2014 (2014), p. 183.

[2] M. Amiri, B. Frauscher, and J. Gotman, *Phase-Amplitude Coupling Is Elevated in Deep Sleep and in the Onset Zone of Focal Epileptic Seizures*, Frontiers in Human Neuroscience, 10 (2016), p. 387.

[3] S. Ashokkumar, M. Premkumar, S. Anupallavi, V. Jeevanantham, G. Mohanbabu, and A. Selvapandian, *Quantifying Functional Connectivity Network Through Synchronization and Graph Theory Approaches for Seizure Prediction*, Wireless Personal Communications, 129 (2023), pp. 213–238.

[4] C. Babiloni, R. Lizio, N. Marzano, P. Capotosto, A. Soricelli, A. I. Triggiani, S. Cordone, L. Gesualdo, and C. Del Percio, *Brain neural synchronization and functional coupling in Alzheimer's disease as revealed by resting state EEG rhythms*, International Journal of Psychophysiology, 103 (2016), pp. 88–102.

[5] O. Bazine, O. Rai, O. Aiadi, R. Hedjam, B. Khaldi, and G. Zhong, *Convolutional cross-modal autoencoder-based few-shot learning for data augmentation with application to alzheimer dementia diagnosis*, Cognitive Computation, 17 (2025), p. 34.

[6] D. Cao, Y. Wang, J. Duan, C. Zhang, X. Zhu, C. Huang, Y. Tong, B. Xu, J. Bai, J. Tong, and Q. Zhang, *Spectral Temporal Graph Neural Network for Multivariate Time-series Forecasting*, in Advances in Neural Information Processing Systems (NeurIPS), vol. 33, 2020, pp. 17766–17778.

[7] D. W. Chadwick, *The treatment of the first seizure: the benefits*, Epilepsia, 49 Suppl 1 (2008), pp. 26–28.

[8] J. Claassen, L. J. Hirsch, K. T. Kreiter, E. Y. Du, E. Sander Connolly, R. G. Emerson, and S. A. Mayer, *Quantitative continuous EEG for detecting delayed cerebral ischemia in patients with poor-grade subarachnoid hemorrhage*, Clinical Neurophysiology, 115 (2004), pp. 2699–2710.

[9] A. Craik, Y. He, and J. L. Contreras-Vidal, *Deep learning for electroencephalogram (EEG) classification tasks: a review*, Journal of Neural Engineering, 16 (2019), p. 031001.

[10] A. Demir, T. Koike-Akino, Y. Wang, M. Haruna, and D. Erdogmus, *EEG-GNN: Graph Neural Networks for Classification of Electroencephalogram (EEG) Signals*, in 2021 43rd Annual International Conference of the IEEE Engineering in Medicine & Biology Society (EMBC), 2021, pp. 1061–1067.

[11] J. S. Fabila-Carrasco, C. Tan, and J. Escudero, *Dispersion entropy for graph signals*, Chaos, Solitons & Fractals, 175 (2023), p. 113977.

[12] J. J. Falco-Walter, I. E. Scheffer, and R. S. Fisher, *The new definition and classification of seizures and epilepsy*, Epilepsy Research, 139 (2018), pp. 73–79.

[13] O. Faust, Y. Hagiwara, T. J. Hong, O. S. Lih, and U. R. Acharya, *Deep learning for healthcare applications based on physiological signals: A review*, Computer Methods and Programs in Biomedicine, 161 (2018), pp. 1–13.

[14] L. Gagliano, A. Chang, L. Shokooh, D. Toffa, F. Lesage, M. Sawan, D. Nguyen, and E. Bou Assi, *Cross-bispectrum connectivity of intracranial EEG: A novel approach to seizure onset zone localization*, in 2023 45th Annual International Conference of the IEEE Engineering in Medicine & Biology Society (EMBC), vol. 2023, 07 2023, pp. 1–4.

[15] N. Ghassemi, A. Shoeibi, M. Khodatars, J. Heras, A. Rahimi, A. Zare, Y.-D. Zhang, R. B. Pachori, and J. M. Gorriz, *Automatic diagnosis of COVID-19 from CT images using CycleGAN and transfer learning*, Applied Soft Computing, 144 (2023), p. 110511.

[16] I. Goodfellow, Y. Bengio, A. Courville, and Y. Bengio, *Deep Learning*, vol. 1, MIT Press, Cambridge, UK, 2016.

[17] A. Hajisafi, H. Lin, Y.-Y. Chiang, and C. Shahabi, *Dynamic GNNs for precise seizure detection and classification from EEG data*, in Advances in Knowledge Discovery and Data Mining (PAKDD), vol. 14648, 2024, pp. 207–220.

[18] A. R. Hassan, S. Siuly, and Y. Zhang, *Epileptic seizure detection in EEG signals using tunable-Q factor wavelet transform and bootstrap aggregating*, Computer Methods and Programs in Biomedicine, 137 (2016), pp. 247–259.

[19] W. A. Hauser and E. Beghi, *First seizure definitions and worldwide incidence and mortality*, Epilepsia, 49 Suppl 1 (2008), pp. 8–12.

[20] R. Hedjam, A. Abdesselam, and F. Melgani, *Change detection from unlabeled remote sensing images using siamese ann*, in IGARSS 2019-2019 IEEE International Geoscience and Remote Sensing Symposium, IEEE, 2019, pp. 1530–1533.

[21] S. Hochreiter and J. Schmidhuber, *Long Short-Term Memory*, Neural Computation, 9 (1997), pp. 1735–1780.

[22] R. Hussein, H. Palangi, R. Ward, and Z. J. Wang, *Epileptic Seizure Detection: A Deep Learning Approach*, arXiv, abs/1803.09848 (2018).

[23] A. Hyafil, *Misidentifications of specific forms of cross-frequency coupling: three warnings*, Frontiers in Neuroscience, 9 (2015), p. 370.

[24] A. Isaksson, *Examples of EEG Signals with Time-varing Spectra Analyzed by Means of a Kalman Filter Method*, Royal Institute of Technology, Stockholm, Sweden, 1975. Technical Report No. 95.

[25] O. Jensen, B. Gips, T. O. Bergmann, and M. Bonnefond, *Temporal coding organized by coupled alpha and gamma oscillations prioritize visual processing*, Trends in Neurosciences, 37 (2014), pp. 357–369.

[26] J. Jirsch and L. Hirsch, *Nonconvulsive seizures: Developing a rational approach to the diagnosis and management in the critically ill population*, Clinical Neurophysiology, 118 (2007), pp. 1660–1670.

[27] A. Karuppasamy, A. Abdesselam, R. Hedjam, H. Zidoum, and M. Al-Bahri, *Recent cnn-based techniques for breast cancer histology image classification*, The Journal of Engineering Research, 19 (2022), pp. 41–53.

[28] K. Kim and H.-S. Oh, *Network time series forecasting using spectral graph wavelet transform*, International Journal of Forecasting, 40 (2024), pp. 971–984.

[29] T. N. Kipf and M. Welling, *Semi-Supervised Classification with Graph Convolutional Networks*, in International Conference on Learning Representations, 2017.

[30] D. Klepl, *Network Inference And Graph Learning in Characterising Alzheimer's Disease*, doctoral thesis, Coventry University, 2024.

[31] D. Klepl, F. He, M. Wu, D. J. Blackburn, and P. G. Sarrigiannis, *Cross-Frequency Multilayer Network Analysis with Bispectrum-based Functional Connectivity: A Study of Alzheimer's Disease*, Neuroscience, 521 (2023), pp. 77–88.

[32] D. Klepl, M. Wu, and F. He, *Graph Neural Network-Based EEG Classification: A Survey*, IEEE Transactions on Neural Systems and Rehabilitation Engineering, 32 (2024), pp. 493–503.

[33] G. Leus, A. G. Marques, J. M. Moura, A. Ortega, and D. I. Shuman, *Graph Signal Processing: History, development, impact, and outlook*, IEEE Signal Processing Magazine, 40 (2023), pp. 49–60.

[34] Q. Li, G. Zhong, C. Xie, and R. Hedjam, *Weak edge identification network for ocean front detection*, IEEE Geoscience and Remote Sensing Letters, 19 (2021), pp. 1–5.

[35] H. Liu, J. Zhang, Q. Liu, and J. Cao, *Minimum spanning tree based graph neural network for emotion classification using EEG*, Neural Networks, 145 (2022), pp. 308–318.

[36] N. Liu, X. He, T. Laurent, F. D. Giovanni, M. M. Bronstein, and X. Bresson, *A General Graph Spectral Wavelet Convolution via Chebyshev Order Decomposition*, in Forty-second International Conference on Machine Learning, 2025.

[37] S. López, G. Suarez, D. Jungreis, I. Obeid, and J. Picone, *Automated Identification of Abnormal Adult EEGs*, in 2015 IEEE Signal Processing in Medicine and Biology Symposium (SPMB), Dec 2015, pp. 1–5.

[38] R. J. Martis, U. R. Acharya, C. M. Lim, K. M. Mandana, A. K. Ray, and C. Chakraborty, *Application of higher order cumulant features for cardiac health diagnosis using ECG signals*, International Journal of Neural Systems, 23 (2013), p. 1350014.

[39] J. A. McEwen and G. B. Anderson, *Modeling the Stationarity and Gaussianity of Spontaneous Electroencephalographic Activity*, IEEE Transactions on Biomedical Engineering, BME-22 (1975), pp. 361–369.

[40] A. V. Medvedev and B. Lehmann, *The classification of absence seizures using power-to-power cross-frequency coupling analysis with a deep learning network*, Frontiers in Neuroinformatics, 19 (2025), p. 1513661.

[41] E. M. Mizrahi and P. Kellaway, *Characterization and classification of neonatal seizures*, Neurology, 37 (1987), pp. 1837–1844.

[42] S. Nadkarni, J. LaJoie, and O. Devinsky, *Current treatments of epilepsy*, Neurology, 64 (2005), pp. S2–S11.

[43] J. Newman, A. Pidde, and A. Stefanovska, *Defining the wavelet bispectrum*, Applied and Computational Harmonic Analysis, 51 (2021), pp. 171–224.

[44] I. Obeid and J. Picone, *The Temple University Hospital EEG Data Corpus*, Frontiers in Neuroscience, 10 (2016), p. 196.

[45] G. Olmos-Garcia de Alba, E. Udaeta Mora, J. Malagon Valdez, D. Villaneuva Garcia, and F. Valarezo Crespo, *Neonatal status epilepticus II: Electroencephalographic aspects*, Clinical EEG, 15 (1984), pp. 197–201.

[46] A. Ortega, P. Frossard, J. Kovačević, J. M. F. Moura, and P. Vandergheynst, *Graph Signal Processing: Overview, Challenges, and Applications*, Proceedings of the IEEE, 106 (2018), pp. 808–828.

[47] C. P. Panayiotopoulos, *Typical absence seizures and related epileptic syndromes: Assessment of current state and directions for future research*, Epilepsia, 49 (2008), pp. 2131–2139.

[48] T.-H. Pham, J. Vicnesh, J. K. E. Wei, S. L. Oh, N. Arunkumar, E. W. Abdulhay, E. J. Ciaccio, and U. R. Acharya, *Autism Spectrum Disorder Diagnostic System Using HOS Bispectrum with EEG Signals*, International Journal of Environmental Research and Public Health, 17 (2020), p. 971.

[49] M. Privitera, M. Hoffman, J. L. Moore, and D. Jester, *EEG detection of nontonic-clonic status epilepticus in patients with altered consciousness*, Epilepsy Research, 18 (1994), pp. 155–166.

[50] A. Romano, S. Alqahtani, J. Griffith, and M. Z. Koubeissi, *Factitious psychogenic nonepileptic paroxysmal episodes*, Epilepsy & Behavior Case Reports, 2 (2014), pp. 184–185.

[51] S. Roy, I. Kiral-Kornek, and S. Harrer, *Deep Learning Enabled Automatic Abnormal EEG Identification*, in 2018 40th Annual International Conference of the IEEE Engineering in Medicine and Biology Society (EMBC), 2018, pp. 2756–2759.

[52] Y. Roy, H. Banville, I. Albuquerque, A. Gramfort, T. H. Falk, and J. Faubert, *Deep learning-based electroencephalography analysis: a systematic review*, Journal of Neural Engineering, 16 (2019), p. 051001.

[53] N. Sabor, Y. Li, Z. Zhang, Y. Pu, G. Wang, and Y. Lian, *Detection of the interictal epileptic discharges based on wavelet bispectrum interaction and recurrent neural network*, Science China Information Sciences, 64 (2021), p. 140406.

[54] S. Schmitt and M. A. Dichter, *Electrophysiologic recordings in traumatic brain injury*, in Traumatic Brain Injury, Part I, J. Grafman and A. M. Salazar, eds., vol. 127 of Handbook of Clinical Neurology, Elsevier, 2015, pp. 319–339.

[55] D. L. Schomer and F. H. L. da Silva, eds., *Niedermeyer's Electroencephalography: Basic Principles, Clinical Applications, and Related Fields*, Oxford University Press, New York, NY, 7th ed., 2018.

[56] V. Shah, E. von Weltin, S. Lopez, J. R. McHugh, L. Veloso, M. Golmohammadi, I. Obeid, and J. Picone, *The Temple University Hospital Seizure Detection Corpus*, Frontiers in Neuroinformatics, 12 (2018), p. 83.

[57] M. Shamsi and F. Marvasti, *Multi-Task Diffusion With Masked Measurements*, IEEE Signal Processing Letters, 32 (2025), pp. 3490–3494.

[58] ——, *Joint Statistical Mask Learning and Distributed Estimation Without Support Priors*, IEEE Transactions on Signal and Information Processing over Networks, 11 (2025), pp. 1127–1137.

[59] V. Sharathappriyaa, S. Gautham, and R. Lavanya, *Auto-encoder Based Automated Epilepsy Diagnosis*, in 2018 International Conference on Advances in Computing, Communications and Informatics (ICACCI), 2018, pp. 976–982.

[60] D. Sharifrazi, R. Alizadehsani, J. Hassannataj Joloudari, S. Shamshirband, S. Hussain, et al., *CNN-KCL: Automatic Myocarditis Diagnosis using Convolutional Neural Network Combined with K-means Clustering*, Preprints, (2020), p. 2020070650.

[61] A. Shoeibi, M. Khodatars, N. Ghassemi, M. Jafari, P. Moridian, et al., *Epileptic Seizures Detection Using Deep Learning Techniques: A Review*, International Journal of Environmental Research and Public Health, 18 (2021), p. 5780.

[62] N. Srivastava and R. Salakhutdinov, *Multimodal learning with Deep Boltzmann Machines*, in Proceedings of the 26th International Conference on Neural Information Processing Systems (NIPS'12), vol. 2, Curran Associates Inc., 2012, pp. 2222–2230.

[63] C. E. Stafstrom and L. Carmant, *Seizures and epilepsy: an overview for neuroscientists*, Cold Spring Harbor Perspectives in Medicine, 5 (2015), p. a022426.

[64] S. Tang, J. Dunnmon, K. Saab, X. Zhang, Q. Huang, F. Dubost, D. L. Rubin, and C. Lee-Messer, *Self-Supervised Graph Neural Networks for Improved Electroencephalographic Seizure Analysis*, in International Conference on Learning Representations (ICLR), 2022.

[65] T.-l. Tao, L.-h. Guo, Q. He, H. Zhang, and L. Xu, *Seizure detection by brain-connectivity analysis using dynamic graph isomorphism network*, in 2022 44th Annual International Conference of the IEEE Engineering in Medicine & Biology Society (EMBC), 2022, pp. 2302–2305.

[66] M. Teplan, *Fundamentals of EEG measurement*, Measurement Science Review, 2 (2002), pp. 1–11.

[67] R. G. Thangarajoo, M. B. I. Reaz, G. Srivastava, F. Haque, S. H. M. Ali, A. A. A. Bakar, and M. A. S. Bhuiyan, *Machine Learning-Based Epileptic Seizure Detection Methods Using Wavelet and EMD-Based Decomposition Techniques: A Review*, Sensors, 21 (2021), p. 8485.

[68] C.-C. Tseng and S.-L. Lee, *Design and Application of Graph Filter Using Orthogonal Jacobi Polynomial*, in 2025 IEEE VTS Asia Pacific Wireless Communications Symposium (APWCS), 2025, pp. 1–5.

[69] I. Tujyinama, B. Abdulrazak, and R. Hedjam, *Multimodal hybrid cnn-transformer with attention mechanism for sleep stages and disorders classification using bio-signal images*, Signals, 7 (2026), p. 4.

[70] J. T. Turner, A. Page, T. Mohsenin, and T. Oates, *Deep belief networks used on high resolution multichannel electroencephalography data for seizure detection*, arXiv, abs/1708.08430 (2017).

[71] A. Vaswani, N. Shazeer, N. Parmar, J. Uszkoreit, L. Jones, A. N. Gomez, L. Kaiser, and I. Polosukhin, *Attention is All you Need*, in Advances in Neural Information Processing Systems (NIPS), vol. 30, Curran Associates, Inc., 2017.

[72] F. Wendling, P. Chauvel, A. Biraben, and F. Bartolomei, *From Intracerebral EEG Signals to Brain Connectivity: Identification of Epileptogenic Networks in Partial Epilepsy*, Frontiers in Systems Neuroscience, 4 (2010), p. 154.

[73] D. Wong, D. Clifton, and L. Tarassenko, *An introduction to the bispectrum for EEG analysis*, in Proceedings of the 5th UK & Republic of Ireland Postgraduate Conference in Biomedical Engineering and Medical Physics (PGBIOMED), Oxford, UK, 2009.

[74] B. Xu, H. Shen, Q. Cao, Y. Qiu, and X. Cheng, *Graph Wavelet Neural Network*, in International Conference on Learning Representations, 2019.

[75] L. Xuyen, T. Le, D. Viet, L. Tran, N. Linh-Trung, and N. Thuan, *Deep Learning for Epileptic Spike Detection*, VNU Journal of Science: Computer Science and Communication Engineering, 33 (2018), pp. 1–13.

[76] C.-H. Yeh, C. Zhang, W. Shi, M.-T. Lo, G. Tinkhauser, and A. Oswal, *Cross-Frequency Coupling and Intelligent Neuromodulation*, Cyborg and Bionic Systems, 4 (2023), p. 0034.

[77] O. Yildirim, M. Talo, B. Ay, U. B. Baloglu, G. Aydin, and U. R. Acharya, *Automated detection of diabetic subject using pre-trained 2D-CNN models with frequency spectrum images extracted from heart rate signals*, Computers in Biology and Medicine, 113 (2019), p. 103387.

[78] D. Yu and L. Deng, *Deep Learning and Its Applications to Signal and Information Processing*, IEEE Signal Processing Magazine, 28 (2011), pp. 145–154.

[79] L. Zhu, L. Mi, C. Zhu, W. Xu, J. Gao, and J. Qu, *Connecting the Patches: Exploring Multi-Scale Relations in Patches via Graph Neural Networks for Short-Term Electricity Load Forecasting*, IEEE Access, 13 (2025), pp. 168287–168304.

[80] K. Zilles, *Brodmann: a pioneer of human brain mapping–his impact on concepts of cortical organization*, Brain, 141 (2018), pp. 3262–3278.